SEMARAK ILMU PUBLISHING

Journal of Advanced Research in Fluid Mechanics and Thermal Sciences

Journal homepage:
https://semarakilmu.com.my/journals/index.php/fluid_mechanics_thermal_sciences/index
ISSN: 2289-7879

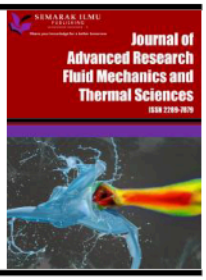


# Numerical Simulations of Base Pressure and Its Control in a Suddenly Expanded Duct at Mach 1.6 using Quarter Circular Ribs

Sayed Ahmed Imran Bellary[1], Ambareen Khan[2], Mohammad Nishat Akhtar[3], Dabir Shahab[4], Sher Afghan Khan[5,*], Khizar Ahmed Pathan[6]

[1] Department of Space Engineering, Ajeenkya DY Patil University, Pune, Maharashtra, India
[2] Centre for Instructional Technology and Multimedia, Universiti Sains Malaysia, Pulau Pinang, Malaysia
[3] School of Aerospace Engineering, Universiti Sains Malaysia, 14300 Nibong Tebal, Pulau Pinang, 11600, Malaysia
[4] Department of Mechanical Engineering, M. H. Saboo Siddik College of Engineering, Mumbai, Maharashtra, India
[5] Department of Mechanical & Aerospace Engineering, Faculty of Engineering, IIUM, Gombak Campus, Kuala Lumpur, Malaysia
[6] Department of Mechanical Engineering, CSMSS Chh. Shahu College of Engineering, Aurangabad, Maharashtra, India

**ARTICLE INFO**

***Article history:***
Received 9 October 2024
Received in revised form 14 January 2025
Accepted 24 January 2025
Available online 20 February 2025

***Keywords:***
Level of expansion; over-expansion; base drag; L/D ratio

**ABSTRACT**

The turbulent flow in a separated region is still a fundamental area of research due to the advent of space shuttles and high-performance military aircraft, and turbulent flow in transonic and supersonic flow is a thrust area for researchers. Whenever the flow experiences an abrupt increase in the area of the enlarged duct, the flow gets significant relief to separate and expand. When the shear layer comes out, it gets divided into two regions: main flow and separated flow. The divided stream line gets reattached with the duct and forms a recirculation zone where the pressure is lower than ambient pressure, resulting in significant drag. This study focuses on base pressure control through quarter-circle rib as a passive control mechanism. Accordingly, a comprehensive numerical simulation was carried out at screech-prone Mach number M = 1.6 for various radii 1 mm, 2 mm, 3 mm, and 4 mm for duct lengths in the range from L = 1D to 6D and nozzle pressure ratios from 3 to 11. Results indicate that for the same range of the rib radius, duct lengths, and level of expansion, there is a progressive increase in the base pressure when rib locations are moved downstream from 0.5D to 3D. The maximum rise in the base pressure is achieved when the rib is located at 66 mm from the base region. A rib with a radius of 1 mm is inadequate for the entire range of rib placement in the present study except when the rib is 11 mm from the base. It can be concluded that a rib of a 1.5 mm radius will be sufficient to neutralize the suction created due to the flow separation. The user can decide on the rib dimension, location, and nozzle pressure ratio based on their requirements.

## 1. Introduction

Sudden flow expansion is a significant issue with many subsonic and supersonic regime applications. An outstanding application of unexpected expansion difficulties is using a jet and shroud combination as a supersonic parallel diffuser. A jet discharging into a shroud and generating a

* *Corresponding author.*
*E-mail address: sakhan@iium.edu.my*

https://doi.org/10.37934/arfmts.127.2.203233

sufficient subatmospheric discharge pressure is another fascinating use, found in the system used to simulate high altitude conditions in jet engine and rocket engine test cells. The exhaust port of an internal combustion engine has a similar flow state; hot exhaust gas jets pass past the exhaust valve. A further pertinent illustration is the flow surrounding the base of a projectile or missile in flight with a blunt edge; in this case, the flow expands inward instead of outward, as in the preceding example.

The physics of the flow, when the shear layer is exhausted in a duct with a more extensive area, would be better understood before analyzing the base pressure data. After leaving the nozzle, the boundary layer will split, expand, and reattach itself to the duct when the Mach number is less than unity. One or more vortices will be present in the separated zone since the first vortex is close to the base and reasonably powerful. It is known as the central vortex. It will function as a pump, moving fluids from the base area to the boundary layer's edge, where the primary jet is located. Low pressure will develop in the recirculation zone due to this pushing activity. Pushing action is too sporadic since this vortex spread is known to occur periodically. This erratic pattern causes variations in the base pressure. But when the tests are being run, it becomes clear that these base pressure changes are minimal. As a result, when evaluating the data, we use the mean base pressure values. The entire flow pattern of the duct may oscillate due to the cyclicity of the vortex desquamation. These oscillations could get very severe regarding geometrical and inertia parameters. The degree of expansion, reattachment length, Mach number, and area ratio are the primary determinants of the intensity of the central vortex located at the base.

The jet that exits the CD nozzle can originate from any of the three situations that are being discussed. Three possible expansions of the flow are optimal: under-, over-, and perfect. Correct expansion will result in an isentropic leaving shear layer dominated by waves that cross the stream flow. A powerful shock wave will be detected when the nozzle experiences negative pressure at the exit. The primary vortex's strength and, thus, the base pressure values will be significantly impacted by this shock, which will cause the flow to shift to the main flow and cause a delay in reattachment and a longer reattachment length.

Last but not least, an expansion fan for under-expanded nozzles speeds up the flow as it expands, causing the flow to diverge in the direction of the base and reattach earlier and with a shorter length. Any ribs present in the duct will produce more vortices. Even though they are tiny, these additional vortices will encourage mixing, raising the base pressure.

The external flow that becomes inward at the expansion point of a blunt-edged projectile or missile during flight presents a dangerous condition. When there is internal flow, the flow exits the nozzle outward and is exhausted into the larger duct. The following are the benefits of studying an abruptly increased flow experimentally with internal rather than exterior flows. By removing the requirement for a tunnel with sufficiently broad cross-sections to ensure that wall interference does not disrupt flow over the model, the size of the air supply required to carry out the experiments is significantly reduced. Along the expansion's entrance section and in the wake area, it is also possible to record the static pressure and surface temperature.

It is well known that the total drag is the sum of skin friction, wave, and base drag. Due to the mission requirement, the skin friction drag will be there by default. Wave drag will exist as and when the Mach number is unity or more than unity. However, while scanning the literature about the wave drag, it is observed, based on several wind tunnel tests, that if the nose finess ratio is 2.5 to 4, the wave drag will be the lowest. Then, the authors are left with the only area to explore: the base pressure control. It is found that the base pressure is lower than atmospheric pressure, which results in a considerable amount of base drag. Literature indicates that the base drag contribution can be up to sixty to seventy percent. Hence, increasing the base pressure by even a tiny amount will significantly decrease the base drag and, thus, the net drag of the missiles, rockets, aircraft bombs,

and shells. This way, we can save fossil fuels, reduce air pollution, and ultimately decrease global warming.

## 2. Literature Review

In this section, literature about base pressure control is discussed. Two methods to control the base pressure are (a) Passive control and (b) Active control. Passive control can be accomplished just by a geometrical alteration, whereas active control requires an external energy source, which is quite challenging to arrange. It may not be so easy to arrange an external source of energy. However, active control has an advantage over passive control, which can be used as and when needed. However, in the case of passive control, the passive control mechanism is in the form of ribs, cavities, vented cavities, after-locked mechanisms, boattails, and step bodies.

Pathan *et al.,* [1,2] underscored the substantial enhancements in base flow characteristics that can be attained through the optimization of expansion geometry; they emphasized the pivotal role of design in augmenting aerodynamic efficacy. In a complementary study, Fiqri *et al.,* [3] investigated control mechanisms within flows that experience sudden expansion and contain cavities at sonic Mach numbers, revealing that strategically designed cavities effectively promote flow reattachment and elevate base pressure, thereby serving as passive control strategies. Asadullah *et al.,* [4] introduced a cost-effective passive method to mitigate base drag, making aerodynamic optimization more feasible and more readily accessible. Pathan *et al.,* [5] delved into the optimization of duct lengths, uncovering their crucial role in enhancing flow management and minimizing pressure losses in expanded flows; this finding further underlines the significance of geometric design considerations.

In the literature, Pathan *et al.,* [6] explored the effects of varying expansion levels on base pressure and reattachment lengths; they discovered that optimized geometries significantly enhance base flow characteristics. Similarly, Azami *et al.,* [7] analyzed supersonic flow dynamics within converging-diverging nozzles, revealing that diverse nozzle configurations can substantially influence flow patterns and facilitate the advancement of passive control techniques for supersonic applications. Furthermore, Pathan *et al.,* [8] illustrated that the optimization of nozzle design, primarily through variations in wall thickness, not only enhances performance but also diminishes structural weight; this underscores the extensive advantages of innovative geometric methodologies within the realm of aerospace engineering. However, the implications of these findings extend beyond mere performance improvements, suggesting a profound impact on future design models.

The research underscores the significance of passive and active control techniques for optimizing flow characteristics in high-speed aerodynamic configurations [9-11]. Passive design strategies, such as meticulously optimized geometries, have consistently demonstrated efficacy in enhancing aerodynamic efficiency without requiring active control mechanisms [12-19]. However, integrating advanced computational tools, such as Computational Fluid Dynamics (CFD), into traditional design frameworks presents substantial challenges, primarily because of fluid dynamics' inherent complexity [20,21].

Computational Fluid Dynamics (CFD) has become an indispensable tool across many applications. Chaudhari *et al.,* [22] elucidated that combustion strategies employed within series catalytic converters significantly influence fluid dynamics, thereby providing critical insights into sonic aerodynamic flows; this revelation is pivotal for advancing the field. Jain *et al.,* [23] illustrated that the orientation of heat sinks markedly affects thermal performance, thus emphasizing the necessity of geometric optimization in heat transfer and flow management. Moreover, Khalil *et al.,* [24] investigated the heat transfer phenomena of air jets, revealing the intricate interplay between airflow dynamics and thermal and aerodynamic designs [24]. Furthermore, they applied CFD

methodologies to enhance flow uniformity within catalytic converters, thereby underscoring its relevance in improving base flow characteristics for aerodynamic applications; however, the implications of these findings extend beyond conventional boundaries [25-28].

Extensive research regarding base pressure control in high-speed flows encompassing passive methodologies such as the implementation of ribs and nozzle optimization further substantiates these findings. Khan *et al.,* [29-31] demonstrated that incorporating quarter and semi-circular ribs within suddenly expanded ducts significantly enhances flow reattachment and diminishes base drag. Similarly, studies conducted by Nurhanis *et al.,* [32] and Khan *et al.,* [33,34] illuminated the critical role of nozzle geometry in stabilizing flow while optimizing base pressure at both sonic and supersonic velocities. Numerical simulations by Khan et al., [35-37] underscored the importance of area ratios in managing flow separation.

Rathakrishnan [38] studied the effect of Rib in a suddenly expanded flow at sonic Mach numbers. He conducted experiments at various nozzle pressure ratios ranging from 1.141 to 2.54 for 3:1, 3:2, and 3:3 rib aspect ratios. His investigation revealed a decreasing trend in the base pressure at a lower aspect ratio, and control decreases the base pressure. The base pressure increased when an aspect ratio of 3:3 Rib was employed. Therefore, depending upon the end user's demands, these combinations of the ribs can be used. If the mission requirement is to increase the base pressure, then the Rib with an aspect ratio is ideal. The Rib with an aspect ratio of 3:1 is the right choice when the application is in a combustion chamber. In the present study, we have validated our CFD results first with the experimental results of Rathakrishnan [38]. After validation, we took various rib geometry, rib location, and nozzle pressure ratios to study passive control's effect on base pressure.

Overall, these studies emphasize the necessity for continued investigation to elucidate the intricate interdependencies inherent in aerodynamic control comprehensively; however, many facets remain unresolved despite the promising advancements achieved thus far.

### *2.1 Literature Gap*

Notwithstanding considerable progress in optimizing base flow characteristics (and passive control strategies), several deficiencies persist within the extant body of research. Although investigations conducted by Pathan *et al.,* [1,2,5,6], Fiqri *et al.,* [3], and Asadullah *et al.,* [4] have elucidated the significance of optimizing expansion geometry and the implementation of strategic cavity designs, a comprehensive analysis regarding the synergistic effects of various passive control methodologies, such as ribs and cavity structures, in complex flow environments across diverse Mach numbers remains conspicuously absent. Moreover, a significant portion of contemporary research underscores the importance of static geometric configurations; however, the potential inherent in adaptive or altering geometries to dynamically optimize flow characteristics remains largely underexplored. Addressing existing gaps will significantly enhance our understanding of intricate aerodynamic phenomena, thus paving the way for developing more robust and adaptive design frameworks within aerospace engineering.

However, these studies show the necessity of continued research in this area, as the interdependencies among various factors remain fully understood. Although promising, this endeavor requires further investigation because the complexities involved are substantial. From the above review, it is evident that there is research on low supersonic Mach numbers, and more so so far, none of the researchers has ever used quarter rib circles as a passive control mechanism. Hence, we intend to study the impact of passive control in the form of a quarter-rib circle. The sharp corner rib will generate secondary vortices, which will interact with duct walls, dividing streamlines, and the main jet to increase the base pressure and decrease the base drag.

## 3. Computational Fluid Dynamic Analysis

### *3.1 Governing Equations*

The following hypotheses are taken into consideration:

i. Turbulent flow is considered because of the turbulent viscous dissipation effects.
ii. The fluid's viscosity varies with temperature and is compressible.
iii. At atmospheric pressure, the flow exits the duct.
iv. While scanning the literature, we found that the internal flow k-epsilon turbulence model is the best as it gives reasonably good results. Shaikh *et al.,* [16] employed the usual k-epsilon turbulence model to simulate internal flow. As a result, the standard k-epsilon turbulence model is applied to the circumstance. Sutherland's three-coefficient viscosity model is expressed as follows:

$$\mu' = \mu'_o \left(\frac{T_a}{T_{a,o}}\right)^{3/2} \frac{T_{a,o}+S\prime}{T_a+S\prime} \tag{1}$$

The reference viscosity value in kg/m-s is denoted as $\mu'$o,, where $\mu'$ represents the viscosity. Ta denotes static temperature, K represents the temperature of a standard reference, and $S'$ is the temperature-dependent Sutherland constant. Three-dimensional continuity equation for compressible flow:

The equation for mass balance is as follows:

$$\frac{\partial \rho}{\partial t} + \underline{\nabla} \cdot (\rho \underline{V}) = 0 \tag{2}$$

where the fluid's velocity is denoted by V.

The equation for momentum balance is:

$$\frac{\partial}{\partial t}(\rho \underline{V}) + \underline{\nabla} \cdot (\rho \underline{\underline{V}}\underline{V}) + \underline{\nabla} p = \underline{\nabla} \cdot \left[2\mu (\underline{\underline{\nabla V}})_o^s\right] + \underline{\nabla} \cdot (\tau_{=Re}) \tag{3}$$

Where $(\underline{\underline{\nabla V}})_o^s = (\underline{\underline{\nabla V}})^s - \frac{1}{3}(\underline{\nabla} \cdot \underline{V})\underline{I}$, $(\underline{\underline{\nabla V}})^s = \frac{\underline{\underline{\nabla V}} + \underline{\underline{\nabla V}}^T}{2}$, and $\tau_{=Re}$ is the turbulent stress tensor.

The formulae for total energy are as follows:

$$\frac{\partial}{\partial t}\left[\rho\left(\frac{1}{2}V^2 + u_{int}\right)\right] + \underline{\nabla}\left[\rho\left(\frac{1}{2}V^2 + u_{int}\right)\underline{V}\right] = \underline{\nabla}\left(\lambda \underline{\nabla} T - p\underline{V} + 2\mu \underline{V} \cdot (\underline{\underline{\nabla V}})_o^s + \underline{V} \cdot \tau_{=Re}\right) \tag{4}$$

where $u_{int}$ is the internal energy, and $\lambda$ is the thermal conductivity.

Many internal flow simulations use the k-epsilon turbulence model due to its affordability, resilience, and sufficient accuracy. The Ansys Fluent program incorporates the k-epsilon ($\varepsilon$) turbulence model used in this research. The K-equation allowed us to calculate the turbulent kinetic energy.

$$\frac{\partial}{\partial t}(\rho k) + \underline{\nabla} \cdot (\rho \underline{V} k) = \underline{\nabla} \cdot \left[(\mu + \frac{\mu_t}{\sigma_k})(\underline{\nabla} k)\right] - \rho\varepsilon + M_x \tag{5}$$

The turbulent kinetic energy dissipation rate is denoted by $\varepsilon$, the turbulent Prandtl number is $\sigma$-$k$, and the word Mx is the turbulence generation. Precisely, the dissipation (or (-equation)) is controlled by,

$$\frac{\partial(\rho\varepsilon)}{\partial t} = -\underline{\nabla}\cdot\left(\rho\varepsilon\vec{V}\right) + \underline{\nabla}\cdot\left[\left(\mu + \frac{\mu_T}{\sigma_\varepsilon}\right)\nabla\varepsilon\right] - C_1 f_1\left(\frac{\varepsilon}{k}\right)M - C_2 f_2\frac{\varepsilon^2}{k} \quad (6)$$

where $\mu_t = \rho f_\mu C_\mu k^2/\varepsilon$ denotes turbulent viscosity, and the arbitrary constants are denoted as $\overline{C_\mu} = 0.09$, $\overline{C_1} = 1.44$, $\overline{C_2} = 1.92$, $\overline{f_\mu} = 1$, $\sigma_k = 1.0$, and $\sigma_\varepsilon = 1.3$.

### *3.2 Geometry and Modelling*

The finite volume technique (FVM) was employed to delve further into this investigation. The CFD simulation used the ANSYS FLUENT 2024/R2 software to assess the nozzle's fluid flows. We are examining the impact of the quarter geometry of the rib in the form of a passive control method. The orientation of the quarter rib is shown in Figure 1.

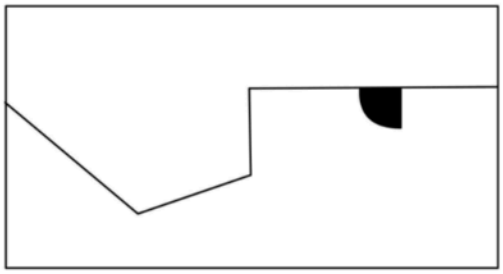

**Fig. 1.** Orientation of the Rib

### *3.3 Meshing and Boundary Conditions*

A crucial part of the CFD process is meshing. By choosing the free-face mesh type, the 2D model is of the structured mesh type in this case. Elements were given sizes according to each line (edge) length when the constructed structured mesh type was used. The lines were utilized to apply the element size, and elements with identical forms were created using face meshing. The mesh independence check is done. Figure 2 below shows the mesh's element type and size tested during mesh independence check.

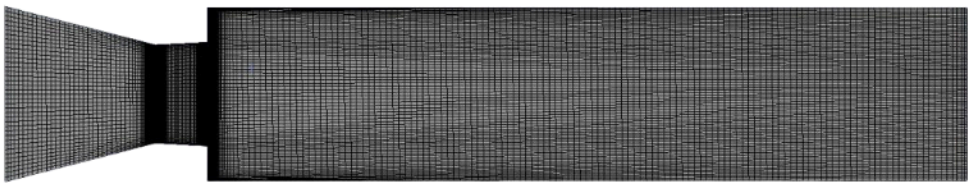

(a)

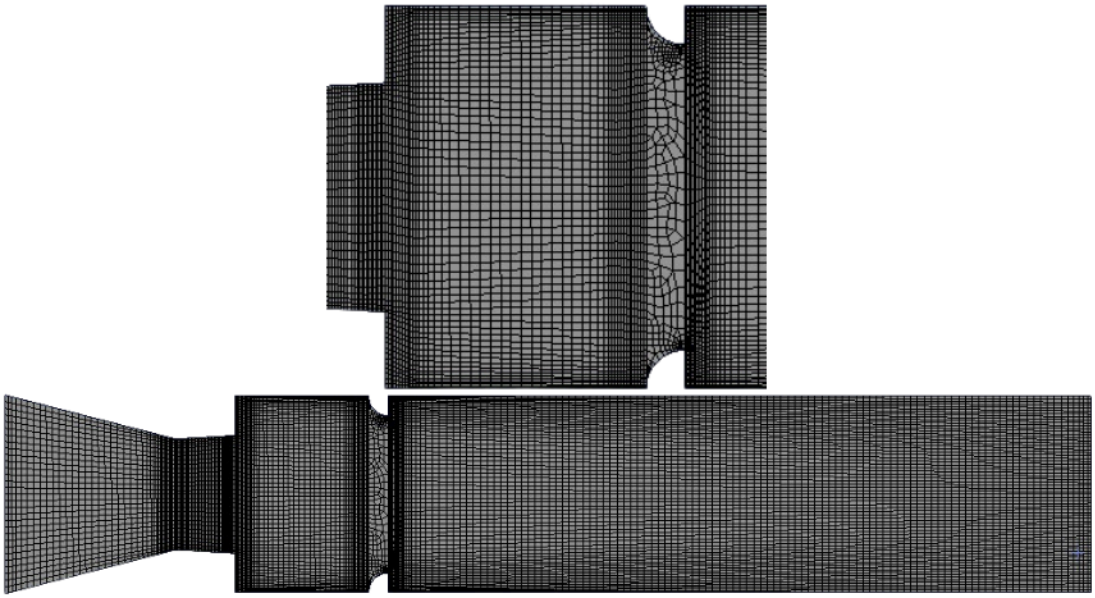

(b)

**Fig. 2.** Mesh model (a) without ribs (b) with ribs

### *3.4 Assumptions and Fluid Properties*

Assumptions are accomplished to replicate the flow activities in the precise physical environment. Appropriate mathematical and numerical models are selected to make simpler the governing equations.

To solve the governing equations simultaneously, numerical modeling requires choosing the appropriate mathematical models, such as the governing equations, boundary conditions, mesh quality, and numerical method. Despite its limitations in accurately representing physical phenomena, the computational method has been trusted for decades and offers sufficient insight into flow behavior. As a result, this calls for careful consideration of elements that closely resemble the flow behavior. This study pinpoints the presumptions that jeopardize the precise physical state. The following are the presumptions and characteristics covered in this study:

The flow is assumed to be a steady 2D flow because geometry is symmetric.

i. The density of the air is variable.
ii. Since turbulent flow has a significant impact on turbulent viscous dissipation at a given flow velocity, it is taken into consideration.
iii. The viscosity of the fluid is dependent on temperature.
iv. At the standard atmospheric pressure, the flows leave the duct. At normal ambient pressure, the flows leave the duct.
v. Since the flow via the nozzle is considered turbulent, the compressible flow field is represented by the k-epsilon standard model. The subsequent equations most appropriately characterize the turbulent flow.

### *3.5 Geometry of the Model*

The ANSYS Workbench program utilized fluid flow (Fluent) analytical techniques and was employed for the entire computational fluid dynamics (CFD) procedure. The model was generated via a Design Modeller. Figure 3 depicts a converging nozzle that abruptly widens into a duct with five ribs. In Rathakrishnan's [38] experimental setup, the dimensions of the convergent-divergent nozzle with a suddenly expanded duct are as stated in Table 1.

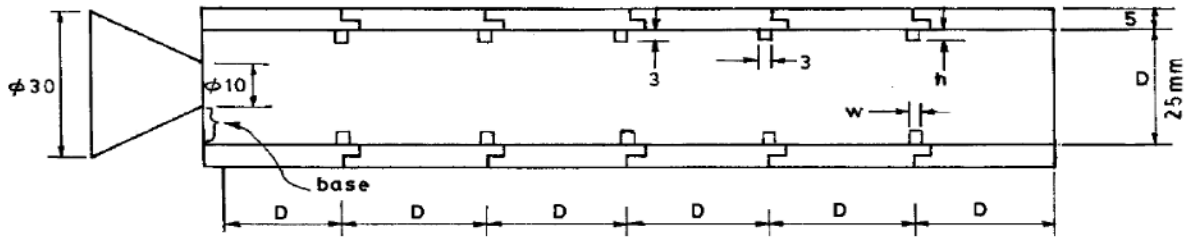


**Fig. 3.** Duct with five ribs used in an experimental study [38]

**Table 1**
The geometries of the validation model

| Parameters | Dimensions |
|---|---|
| Nozzle inlet diameter | 30 mm |
| Nozzle outlet diameter | 10 mm |
| Duct diameter | 25 mm |
| Duct length | Varies from 1D to 6D |
| Converging length | 20 mm |
| Rib width | 3 mm |
| Rib height | Varies from 1mm to 3mm |

### *3.6 Validation of Previous Work*

According to Rathakrishnan [38], the prior work was performed at aspect ratios of 3:3, 3:2, and 3:1; an area ratio of 6.25; L/D ranging from 1 to 6; pressure ratios of 1.141, 1.295, 1.550, 1.707, and 2.458; and nozzle exit Mach numbers of 0.44, 0.62, 0.82, 0.91, and 1.0. However, in a prior publication by Rathakrishnan [38], the result from Figure 4 with NPR ($P_{01}/P_a$) 2.458 and models with control in the form of ribs with 3:2 and 3:3 aspect ratios was chosen to be compared to the current work. The simulation is supported by Rathakrishnan's [38] experimental work, which used five ribs positioned at equidistant intervals in the duct, as illustrated in Figure 3. The results of base pressure fluctuation with NPR of 2.458 and L/D ranging from 2 to 6 are obtained. The study is repeated to validate the numerical results of a model with control over different rib aspect ratios.

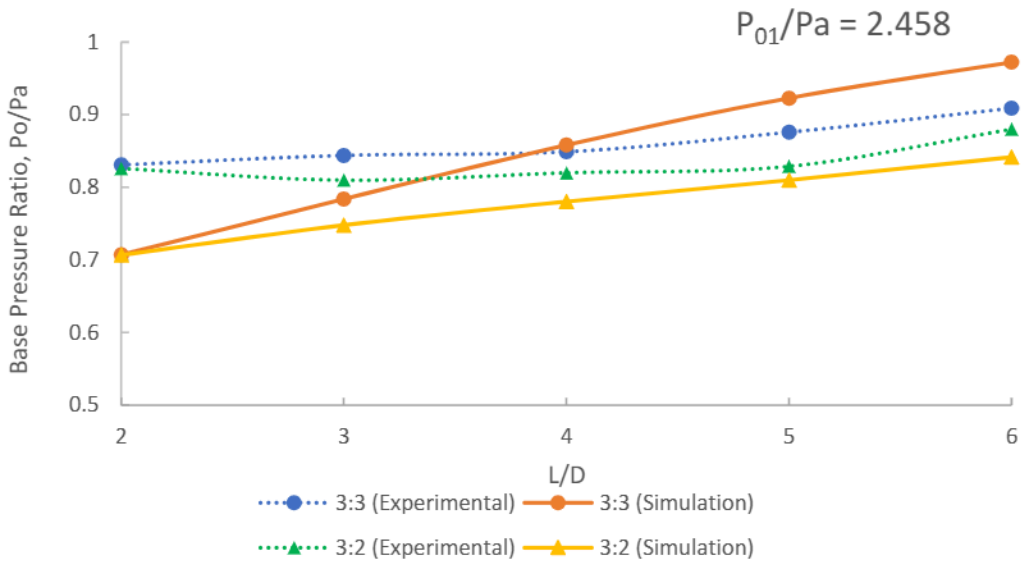


**Fig. 4.** Validation of previous work by Rathakrishnan [38]

Figure 4 demonstrates the current and earlier studies' base pressure ratio data curves [38]. The experimental values were denoted by dotted lines, while the simulation results obtained using ANSYS Fluent were represented by straight lines. The present numerical analysis exhibited a percentage discrepancy of less than 10% compared to the previous experimental study. Consequently, the current work met the criteria for acceptability. The curves exhibited a consistent pattern, with each point close to the subsequent one. As a result, based on the table and graph described before, the validation of the current work was successful.

### *3.7 Mesh Independence Study*

Table 2 provides data from a mesh independence study, a crucial step in computational simulations to ensure that the results remain consistent regardless of the mesh refinement level. The element sizes range from the coarsest to the finest, with corresponding node and element counts for each mesh configuration. As the mesh becomes finer, the number of nodes and elements increases significantly, from 1,284 nodes and 1,145 elements in the coarsest mesh to 1,354,262 nodes and 1,351,303 elements in the finest mesh.

This study aims to determine the optimal mesh size for accurate simulations without unnecessary computational expense. The table shows a notable increase in nodes and elements as the mesh is refined. The coarsest mesh has relatively few nodes and elements, which means lower computational cost but potentially less accuracy. Conversely, the finest mesh offers the highest resolution at the expense of significant computational resources. The medium and fine meshes provide intermediate levels of refinement, offering a balance between accuracy and efficiency.

Based on the node and element numbers trends, the finest mesh will likely produce the most accurate results (Figure 5). However, continuing to refine the mesh beyond a certain point may offer diminishing returns in terms of accuracy while significantly increasing computational time. A critical assessment of this table would suggest that the "Fine" or "Finer" mesh configurations may represent the best balance between accuracy and computational efficiency. These configurations substantially increase nodes and elements compared to the medium meshes without reaching the computational expense of the finest mesh. If simulation results do not significantly change between the fine and finest meshes, further refinement to the finest mesh is unnecessary, as it would only increase

computational time without added benefit. Thus, the fine or finer mesh sizes are likely the best choices for further simulation.

**Table 2**
Mesh independence study

| Element size | Coarsest | Coarse | Medium 1 | Medium 2 | Fine | Finer | Finest |
|---|---|---|---|---|---|---|---|
| Nodes | 1284 | 1933 | 7490 | 15240 | 124938 | 359022 | 1354262 |
| Elements | 1145 | 1777 | 7237 | 14895 | 124008 | 357492 | 1351303 |


**Fig. 5.** Results of mesh check

## 4. Results and Discussion

It would be better to understand the flow mechanics when the shear layer is exhausted in a duct with a more significant area before analyzing the base pressure results caused by the ribs. The boundary layer will detach, expand, and rejoin the enlarged duct when it exits the nozzle when the Mach number is less than unity. The separated region will have one or more vortices because the initial vortex is near the base and relatively robust. The central vortex is the name given to this vortex. Fluids will be transferred from the base region to the main jet on the boundary layer's edge, employing this device operating as a pump. The recirculation zone will experience low pressure due to this pushing action. But pushing activity is too sporadic since, as we know, this vortex spread is a periodic phenomenon. The base pressure fluctuates as a result of this erratic pattern.

Nevertheless, it was found that these base pressure differences are minimal when the tests are done. As a result, we use the mean base pressure values while evaluating the data. The whole flow pattern in the larger image may be oscillatory due to the cyclicity of the vortex desquamation. For geometrical and inertia values, these oscillations have the potential to become extremely severe. The core vortex at the base's intensity is determined mainly by the area ratio, Mach number, reattachment length, and degree of expansion.

Analyzing the flow mechanics would be a better place to start when examining the base pressure results induced by the ribs when the shear layer is exhausted in a duct with a larger area. The boundary layer appears from the nozzle, spreads, and reattaches to the expanded duct when the Mach number is less than unity. Since the initial vortex is near the base and sufficiently robust, one or more vortices will be in the separated zone. We call it the core vortex. It will move fluids from the base area to the edge of the boundary layer, where the primary jet is situated, acting as a pump. This pushing action will build up low pressure in the recirculation zone. Since this vortex spread is known to happen occasionally, the pushing motion is too erratic. The base pressure varies as a result of this unpredictable pattern. However, it is evident from the testing that these base pressure variations are negligible. Therefore, we use the mean base pressure values while analyzing the data. The cyclicity of the vortex desquamation suggests that the entire flow pattern in the enlarged image could be oscillatory. Concerning geometrical and inertia parameters, these oscillations have the potential to become extremely severe. The main factors that determine the intensity of the central vortex at the base are the degree of expansion, reattachment length, Mach number, and area ratio.

Figure 6 shows a view of the converging-diverging nozzle with duct and quarter-circle rib for orientation one. The figure shows that the curved part faces the flow from the nozzle first, whereas the straight part of the rib is demonstrated towards the trailing edge.

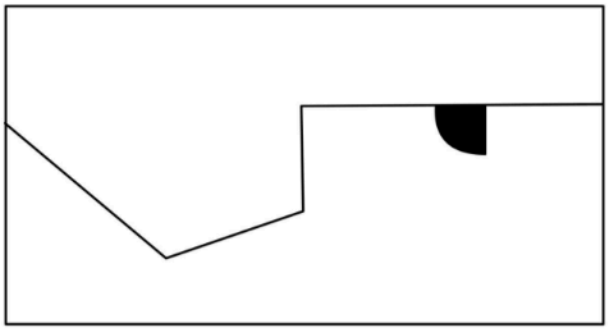

**Fig. 6.** A view of the Nozzle, duct, and rib Assembly

To alter the base pressure, quarter-circle ribs installed in the ducts are the subject of this investigation's efficiency analysis. The area ratio, the duct's L/D ratio, the Mach number, and the level of expansion (NPR) are the characteristics considered in this study. Through division by the atmospheric pressure, the recorded base pressures are normalized.

For NPRs ranging from 3 to 11, the base pressure dependence for area ratios of 4.84 is presented. Base pressure outcomes are contrasted with and without treatment. These results demonstrate the base pressure's reliance on the Mach number in the supersonic region. The control effectiveness for a given Mach number mostly depends on the nozzle pressure ratio (NPR), which determines the amount of expansion. Furthermore, increasing NPR enhances the control's ability to raise base pressure. This trend might result from the shock at the nozzle exit, which weakens the vortex at the base by turning the flow away from the base region.

The oblique shock at the nozzle exit may become milder than that at lower NPRs due to the decrease in overexpansion as the NPR rises. The vortex is thus nearly intact as the tendency to divert the incoming flow decreases. Under these circumstances, passive control can cause them to spread without any propensity to deflect, entraining some mass from the standing vortex and convecting it away from the base, raising the base pressure above those without control. For Mach 1.6, the NPR needed for correct expansion is 4.25. Meanwhile, the simulations are done for NPRs ranging from 3 to 11, resulting in expansion levels of 0.71, 1.18, 1.65, 2.12, and 2.6. This level of expansion indicates that flow from the nozzle while exiting from the nozzle undergoes over-expansion, correct expansion,

and under-expansion. At NPR = 3, the jet is over-expansion; for remaining NPRs, the nozzle remains under-expansion, and the level of under-expansion increases with an increase in the NPR values.

### *4.1 Base Pressure Results for Rib Location at 0.5D*

Figure 7(a) to Figure 7(f) show the outcome of this study when a quarter-circle rib is placed at 11 mm from the base inside the duct, various radii ranging from 1 mm to 4 mm at different expansion levels for duct lengths in the range L = 1D to 6D. As we know, at Mach M = 1.6, only at NPR = 3, the jets are over-expanded, and for the rest of the NPRs, the nozzle exhausting the shear layer into the enlarged duct remains under-expanded. That implies that when the nozzle is over-expanded, the pressure at the nozzle lip will be less than the ambient pressure, and this pressure has to become equal to the ambient pressure, and it will be possible when the flow passes through the oblique shock waves. When the flow exits from the nozzle and starts interacting with the waves, this process will continue till the flow attains ambient pressure.

From Figure 7(a), it is seen that there is a decrease in the base pressure without control or when a 1 mm radius rib is employed, and once the nozzle is under-expanded, this decreasing trend gets arrested, and there is a progressive rise in the base pressure. Furthermore, when we look at the results for rib radii 2 mm, 3 mm, and 4 mm, it is found that the declining trend in the base pressure is absent, rather than there is a linear increase in the base pressure once the rib radius is 2 mm and above. Even without a control case, the base pressure recovery takes place, and there is still a difference of 40%. For this duct length L = 22 mm, when ribs of radii 1 mm, 2 mm, 3 mm, and 4 mm are employed, the Base pressure ratios are 0.95, 1.3, 1.7, and 2.3, respectively. Since the duct length is small and flow will not be attached to the duct wall, these results are unreliable due to the influence of ambient pressure.

Figure 7(b) shows base pressure results for duct length L = 44 mm at various rib radii and NPRs. Results indicate that the impact of a rib with a radius of 1 mm is not visible for this duct length, and base pressure values with and without control are the same. The physics behind this trend may be due to the increased duct length from 22 mm to 44 mm, significantly decreasing the backpressure's impact. However, for ribs with a radius of 2 mm to 4 mm, the base pressure results are nearly the same as in the previous case; it may be due to the increase in the rib radius, and the secondary vortices formed will push more mass towards the base. Hence, there is a significant rise in the base pressure.

Figure 7(c) to Figure 7(d) shows similar results for duct lengths L = 66 mm and 88 mm, except for rib radius 1 mm; we observe some fluctuation in base pressure, and this change is due to the duct length and influence of the back pressure. When we look for duct lengths L = 110 mm and 132 mm, they too represent similar except for a marginal reduction in the magnitude of the base pressure due to the considerable increase in the duct length, resulting in a minimum influence of ambient pressure inside the duct flow field.

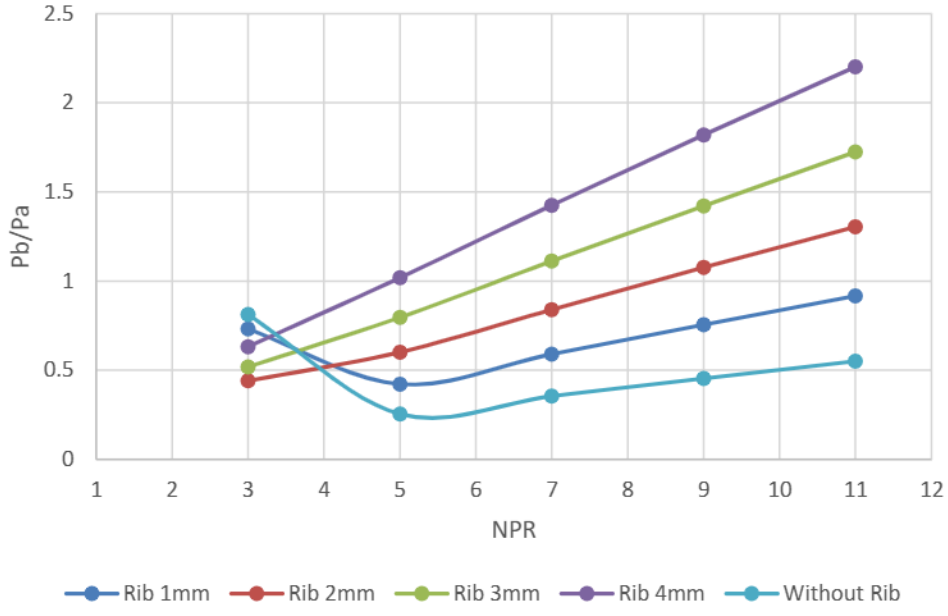
2.5
2
1.5
1
0.5
0
Pb/Pa
1
2
3
4
5
6
7
8
9
10
11
12
NPR
Rib 1mm
Rib 2mm
Rib 3mm
Rib 4mm
Without Rib

(a) L/D = 1

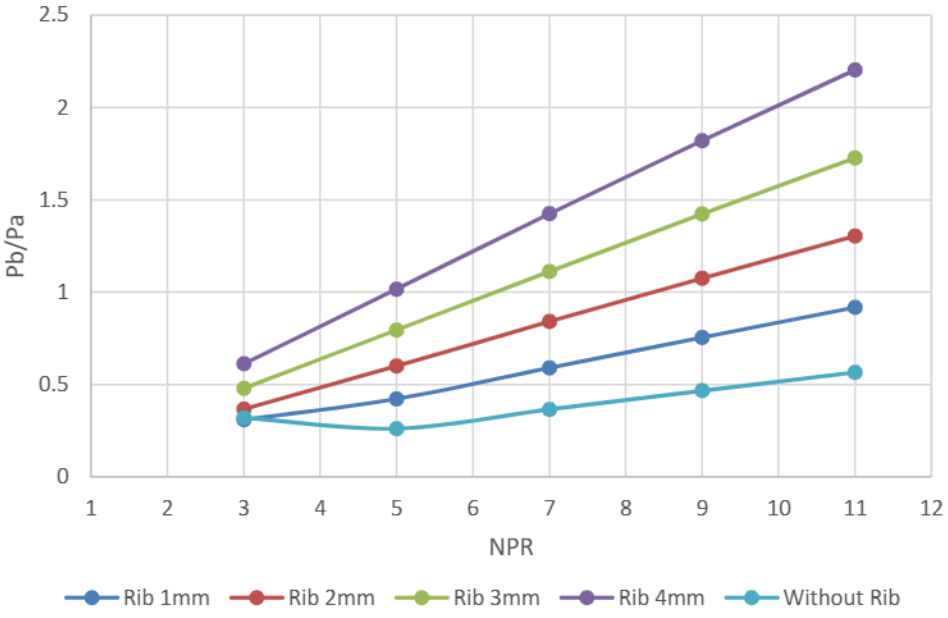
2.5
2
1.5
1
0.5
0
Pb/Pa
1
2
3
4
5
6
7
8
9
10
11
12
NPR
Rib 1mm
Rib 2mm
Rib 3mm
Rib 4mm
Without Rib

(b) L/D = 2

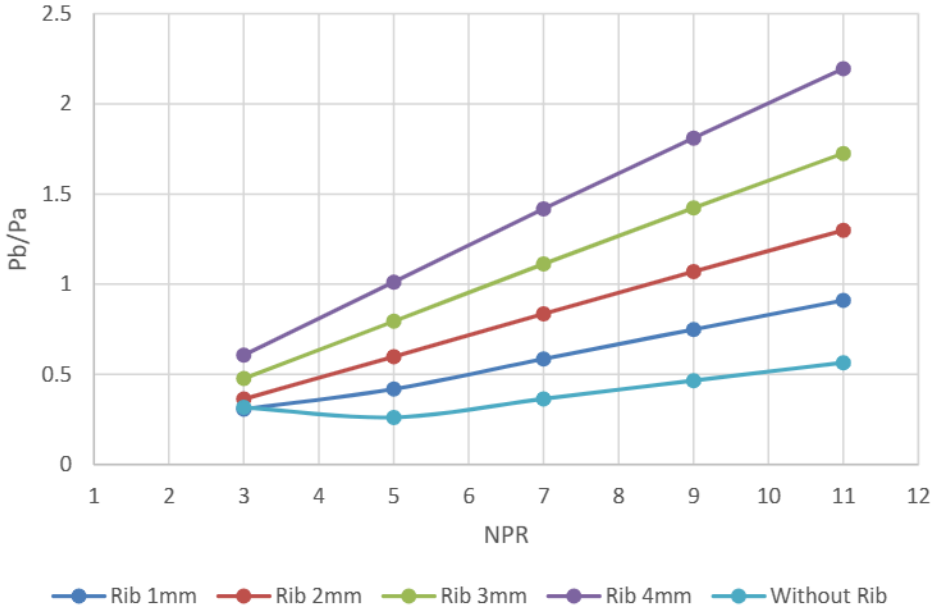
2.5
2
1.5
1
0.5
0
Pb/Pa
1
2
3
4
5
6
7
8
9
10
11
12
NPR
Rib 1mm
Rib 2mm
Rib 3mm
Rib 4mm
Without Rib

(c) L/D = 3

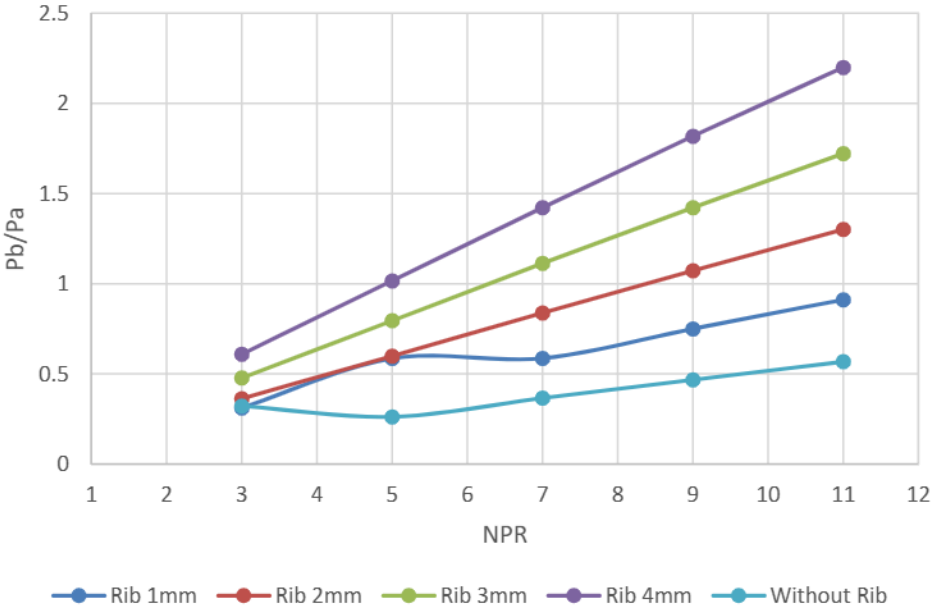
2.5
2
1.5
1
0.5
0
Pb/Pa
1
2
3
4
5
6
7
8
9
10
11
12
NPR
Rib 1mm
Rib 2mm
Rib 3mm
Rib 4mm
Without Rib

(d) L/D = 4

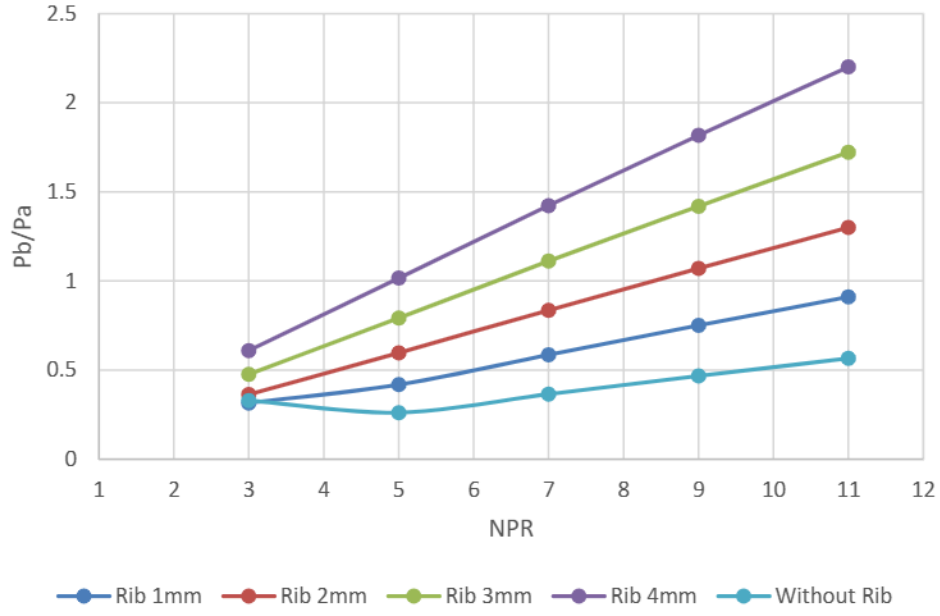


(e) L/D = 5

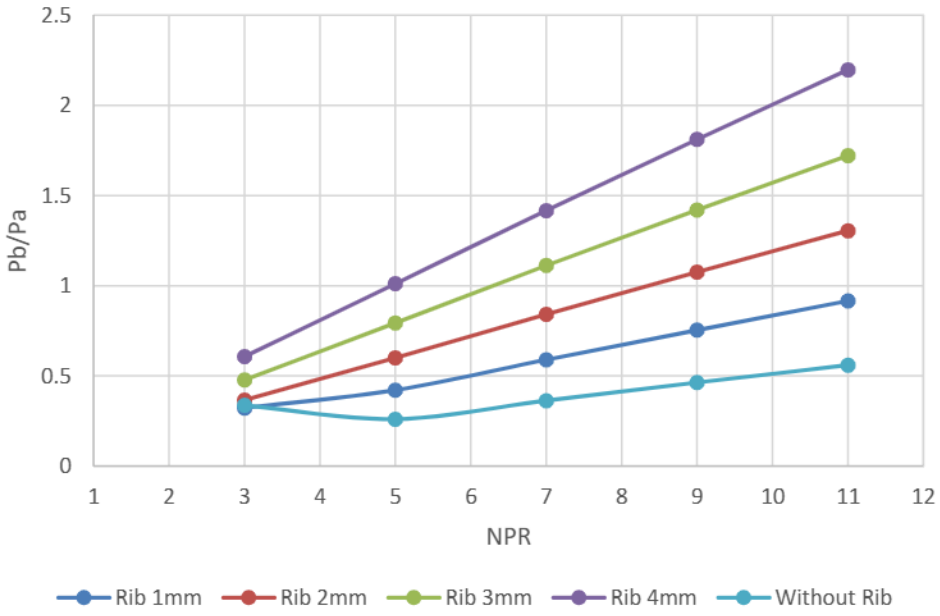


(f) L/D = 6

**Fig. 7.** Base Pressure Vs. NPR for various duct lengths

### *4.2 Base Pressure Results for Rib Location 1D*

Figure 8(a) to Figure 8(e) depict the findings of this study when ribs are placed at 22 mm from the base for four radii of the ribs, namely 1 mm, 2 mm, 3 mm, and 4 mm, for duct lengths in the range from 22 mm to 132 mm and at various levels of expansion having nozzle pressure ratios (NPRs) in the range 3 to 11. From the figure, we may draw the following inferences: Because the shift in the rib location does not yield any positive results, the base pressure values remained in the same range as was seen in the previous case, where ribs were located 11 mm from the base. We anticipate the following reasons for these unchanged base pressure value trends. One of the primary reasons could be the high Mach number, which plays a vital role in fixing the base pressure values. When the shear layer interacts with the rib surfaces in the presence of either an oblique shock wave or an expansion fan, the rib location is nowhere near the reattachment point. For lower duct sizes, the ambient

pressure will impact the flow field inside the duct. It is also seen that there is a marginal decrease in the base pressure for smaller duct sizes for a rib radius of 1 mm and 3 mm.

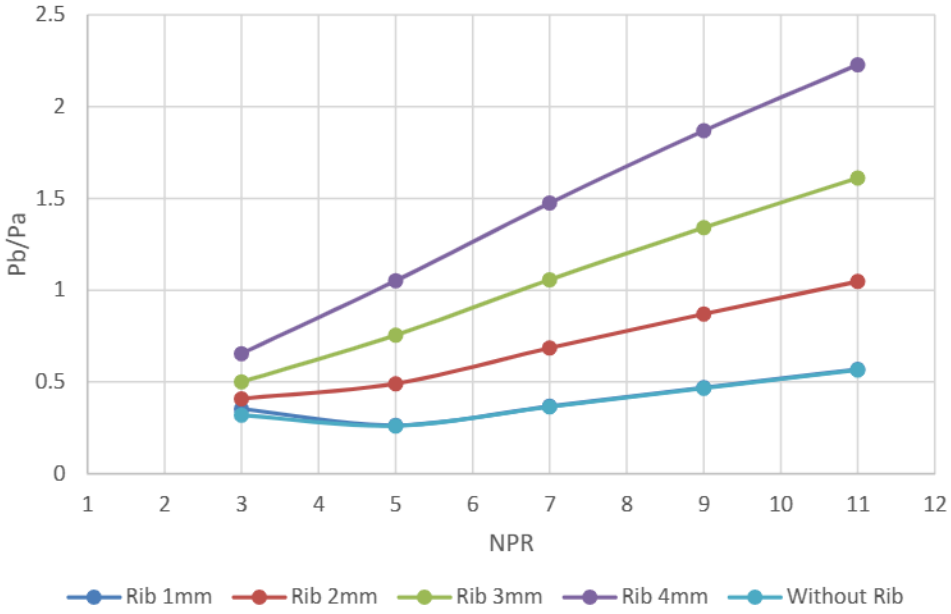


(a) L/D = 2

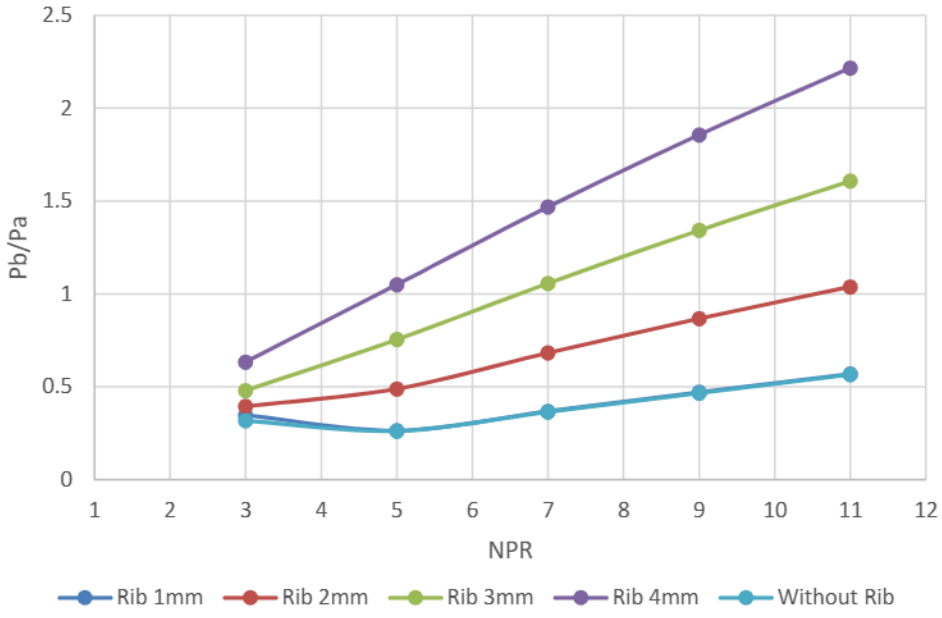


(b) L/D = 3

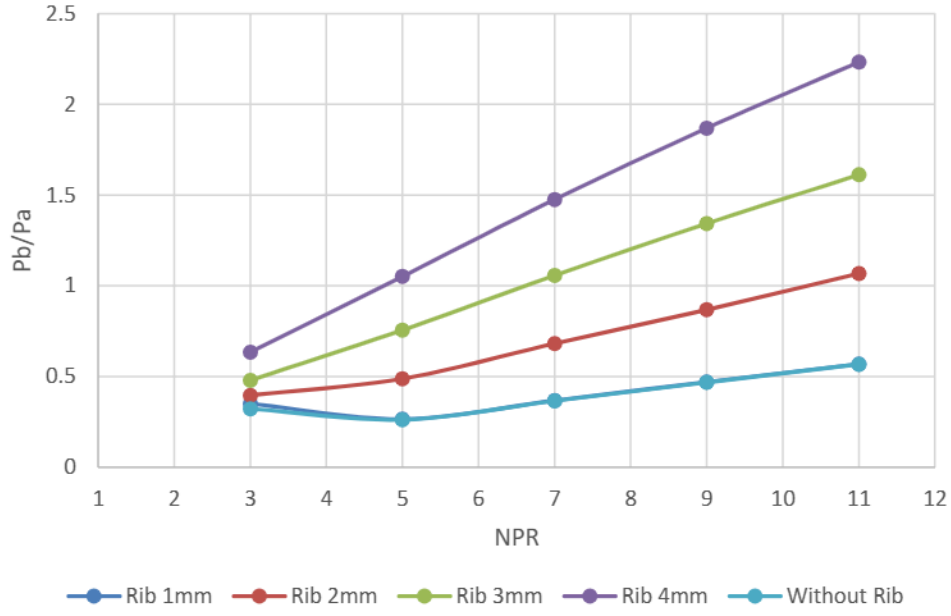
2.5
2
1.5
1
0.5
0
Pb/Pa
1
2
3
4
5
6
7
8
9
10
11
12
NPR
Rib 1mm
Rib 2mm
Rib 3mm
Rib 4mm
Without Rib

(c) L/D = 4

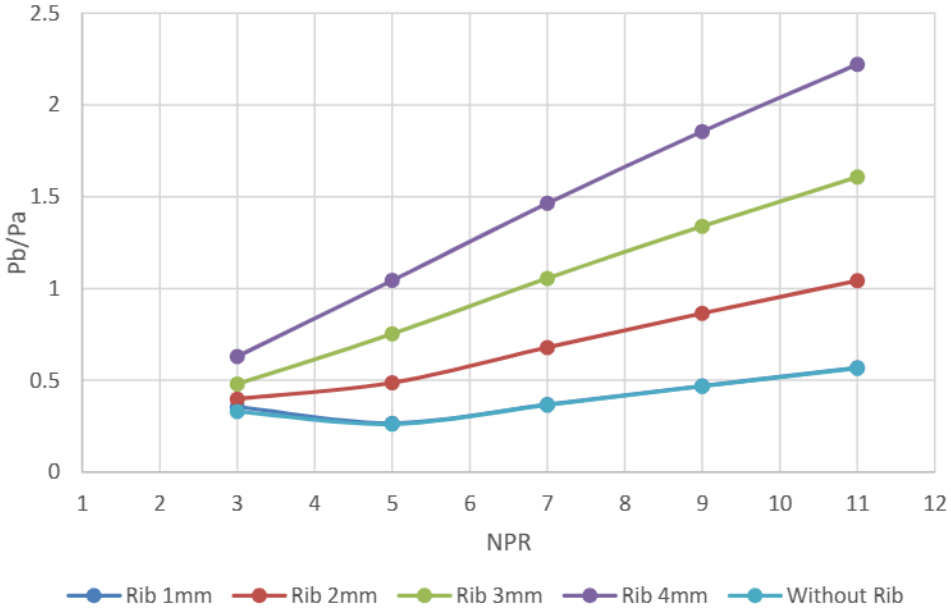
2.5
2
1.5
1
0.5
0
Pb/Pa
1
2
3
4
5
6
7
8
9
10
11
12
NPR
Rib 1mm
Rib 2mm
Rib 3mm
Rib 4mm
Without Rib

(d) L/D = 5

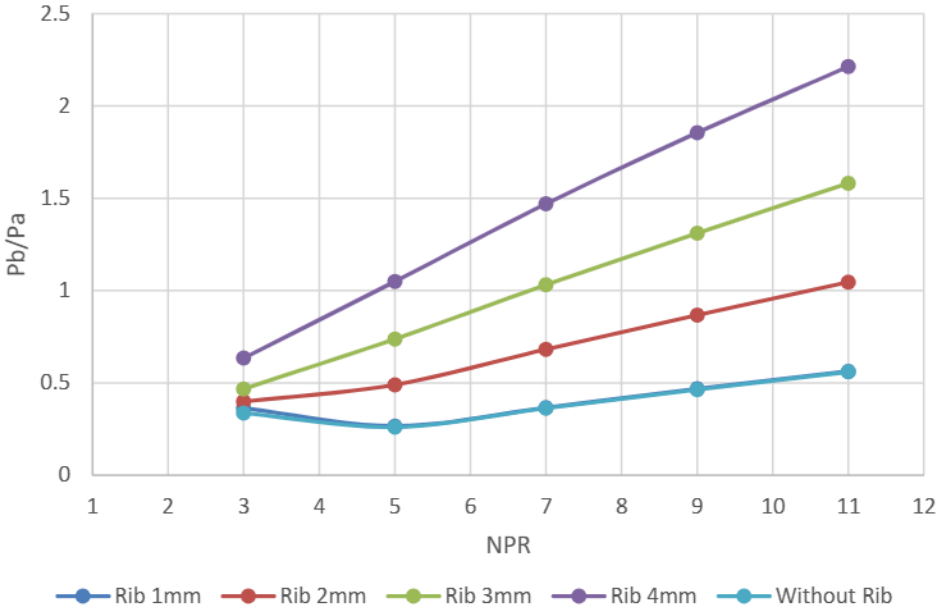


(e) L/D = 6

**Fig. 8.** Base Pressure Vs. NPR for various duct lengths

### *4.3 Base Pressure Results for Rib Location 1.5D*

Figure 9(a) to Figure 9(e) show the outcomes of this study when the control is employed at a distance of 33 mm from the base for various rib radii, duct length ranging from L = 22 mm to 132 mm, at various expansion level for the NPRs in the range 3 to 11. The results show that the 1 mm rib has a marginal impact as a control mechanism in the NPRs from 3 to 5 when nozzles are over-expanded. It is also seen that with an increase in the duct lengths, there is a minor change in the base pressure magnitude. These minor changes in the base pressure can be attributed to the fact that there is a change in the duct length, for lower duct length flow may not be attached to the wall of the duct, and based on the results obtained, one can state that minimum duct length needed is 66 mm. Furthermore, the ambient pressure will also influence the flow field inside the duct, and the back pressure will not significantly impact the duct's flow field for duct lengths 110 mm and 132 mm. The overall base pressure ratios for the present set of parameters at the highest value of NPR of simulation are 2.9, 2, 1.5. and 0.6 for rib radii 1 mm, 2mm, 3mm, and 4 mm.

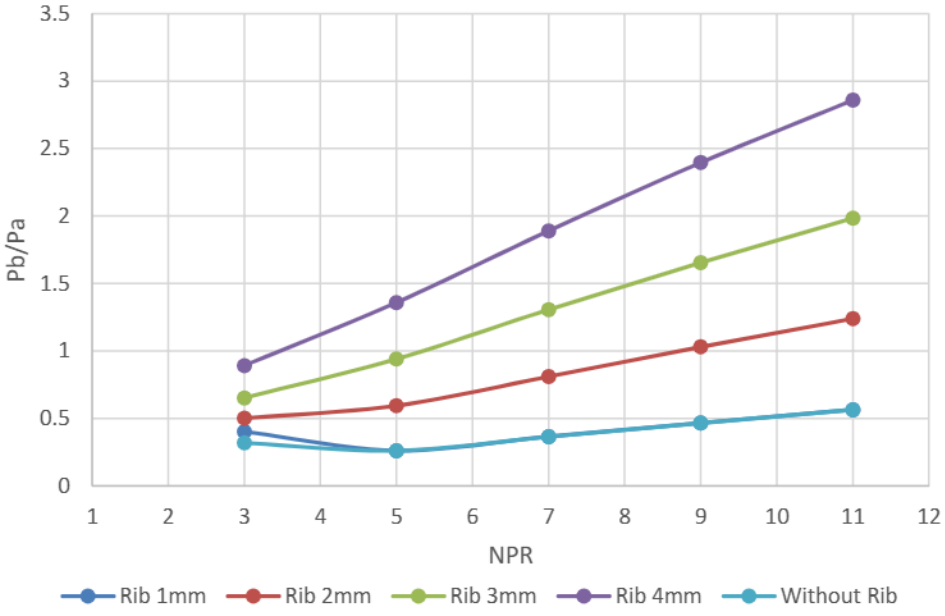
3.5
3
2.5
2
1.5
1
0.5
0
Pb/Pa
1
2
3
4
5
6
7
8
9
10
11
12
NPR
Rib 1mm
Rib 2mm
Rib 3mm
Rib 4mm
Without Rib

(a) L/D = 2

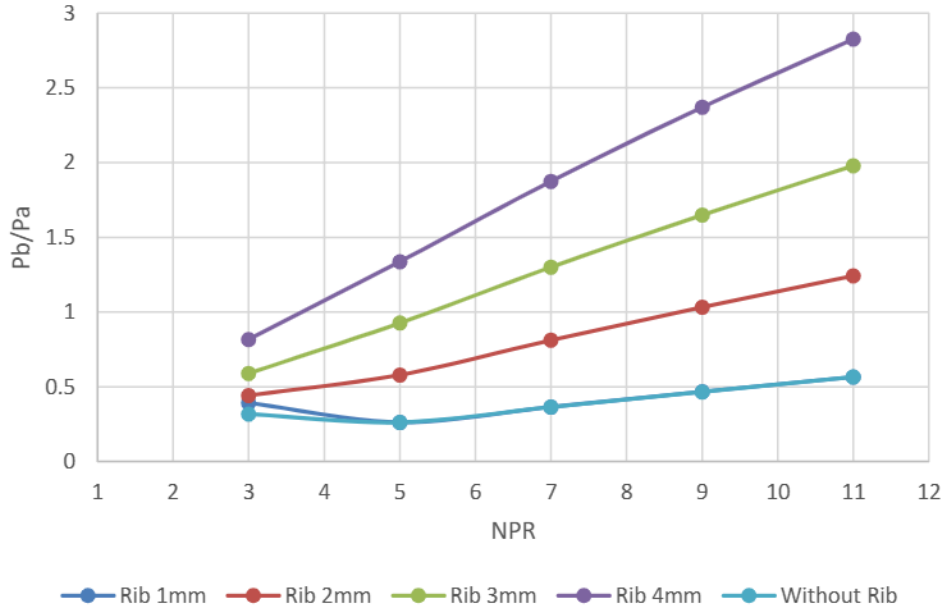
3
2.5
2
1.5
1
0.5
0
Pb/Pa
1
2
3
4
5
6
7
8
9
10
11
12
NPR
Rib 1mm
Rib 2mm
Rib 3mm
Rib 4mm
Without Rib

(b) L/D = 3

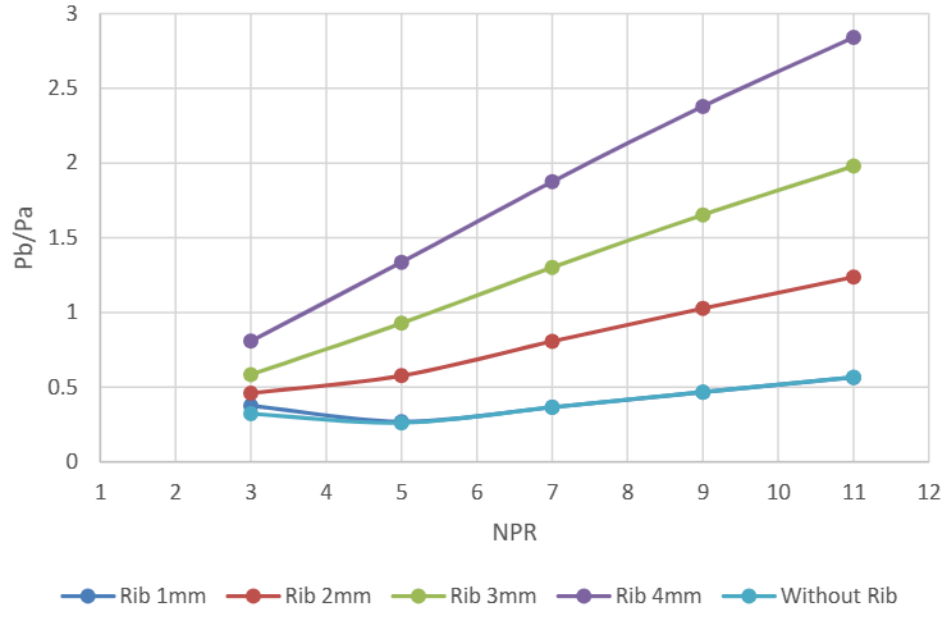
Pb/Pa
NPR
Rib 1mm
Rib 2mm
Rib 3mm
Rib 4mm
Without Rib

(c) L/D = 4

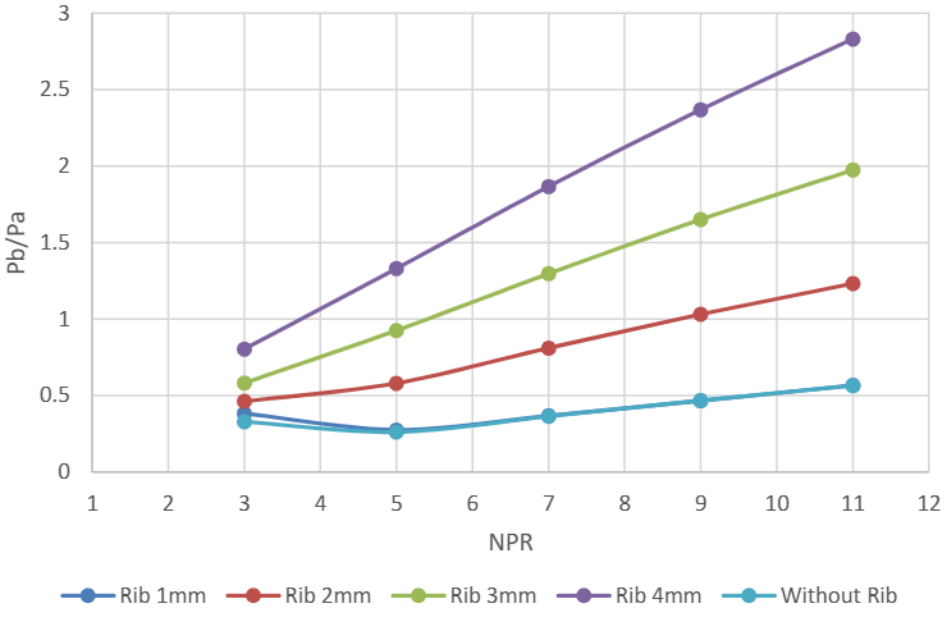
Pb/Pa
NPR
Rib 1mm
Rib 2mm
Rib 3mm
Rib 4mm
Without Rib

(d) L/D = 5

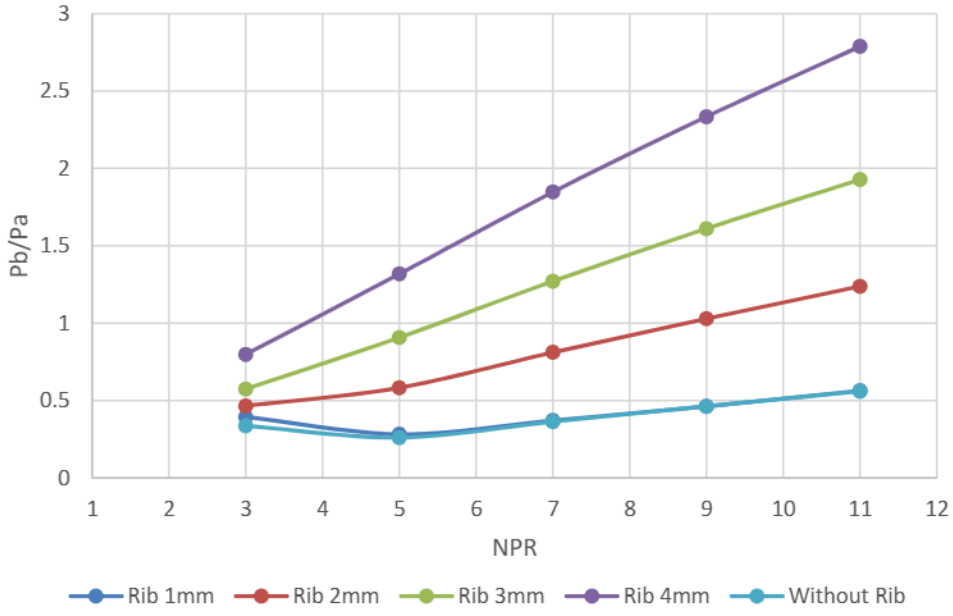


(e) L/D = 6

**Fig. 9.** Base Pressure Vs. NPR for various duct lengths

### *4.4 Base Pressure Results for Rib Location 2D*

The outcomes of this numerical study show ribs of different radii, various duct lengths, and nozzle pressure ratios ranging from 3 to 11 in Figure 10(a) to Figure 10(d). As observed in the previous cases of duct lengths, there are variations in the base pressure for NPR in the range of 3 to 5 only and later, and the base pressure values are the same for 1 mm rib radius and in the absence of the ribs. This trend may be due to the jets being over-expanded in this range of NPR, and for NPRs beyond this range, the nozzle is facing a favorable pressure gradient. We know that whenever controls are employed, active or passive, they become effective once the nozzles are flowing under the influence of a favorable pressure gradient. In the present case, the NPR needed for correct expansion is 4.25; hence, any NPR larger than 4.25 will turn jets under-expanded, and a further increase in the NPR will increase the under-expansion level. According to this analysis, the base pressure ratios for various rib radii, namely 2 mm, 3 mm, and 4 mm, are 1.4, 2.2, and 3.4, as seen in Figure 10(a). Similar trends are seen for other duct lengths as all the parameters are the same except the duct length variation from L = 3D to 6D. Due to this change in the duct length, the influence of the atmospheric pressure will have the least impact on the flow field of the duct, and the same is reflected in the result with minor variations in the base pressure ratio.

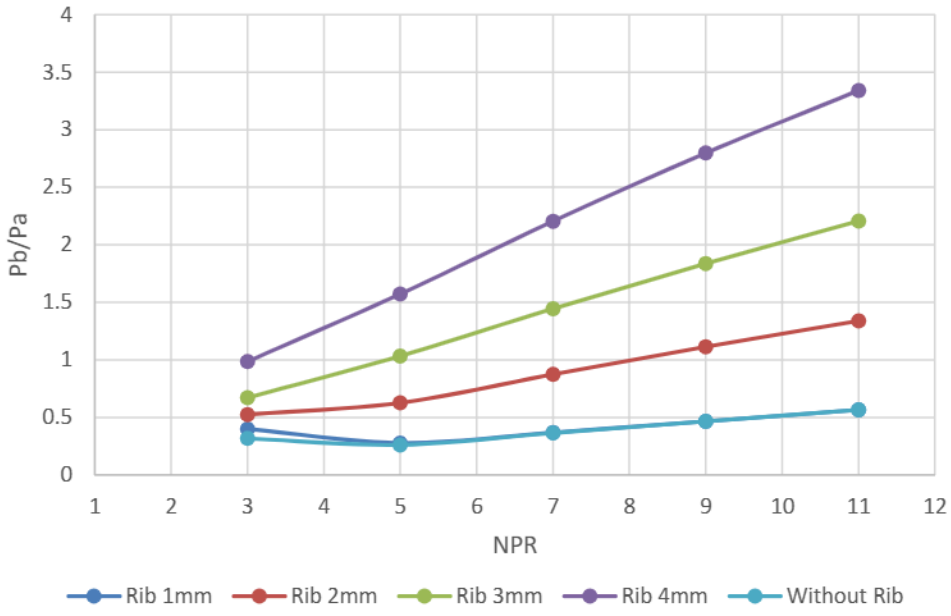
Pb/Pa
NPR
Rib 1mm
Rib 2mm
Rib 3mm
Rib 4mm
Without Rib

(a) L/D = 3

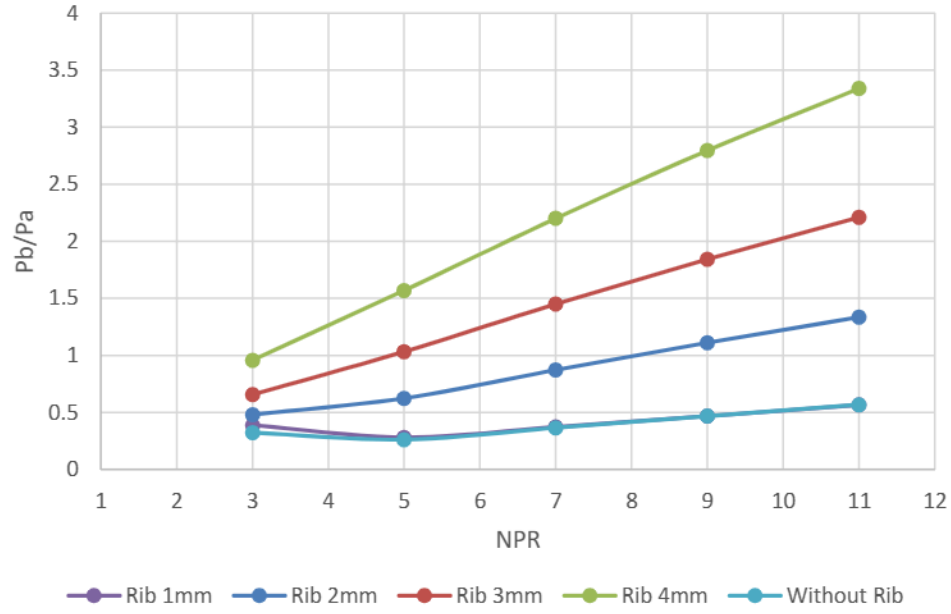
Pb/Pa
NPR
Rib 1mm
Rib 2mm
Rib 3mm
Rib 4mm
Without Rib

(b) L/D = 4

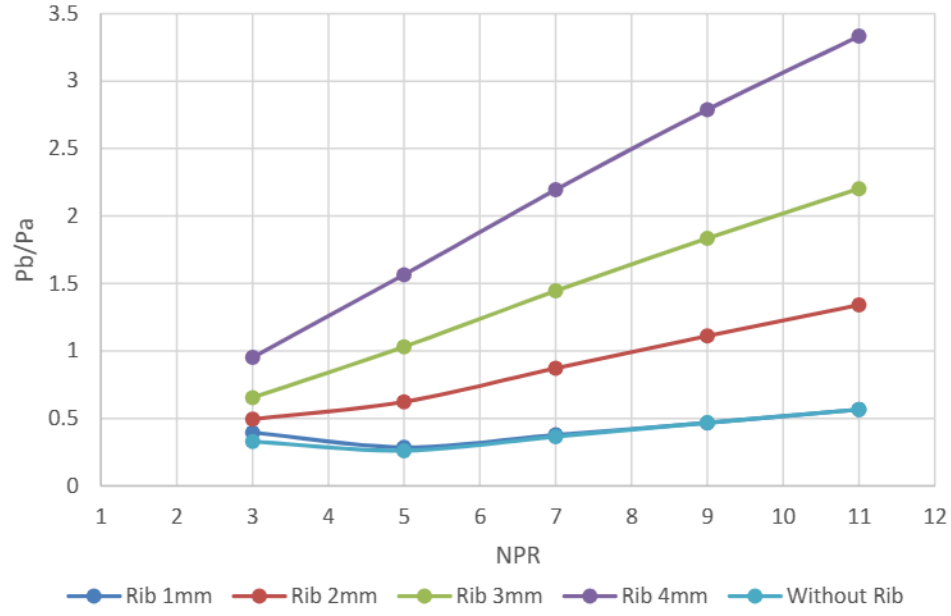


(c) L/D = 5

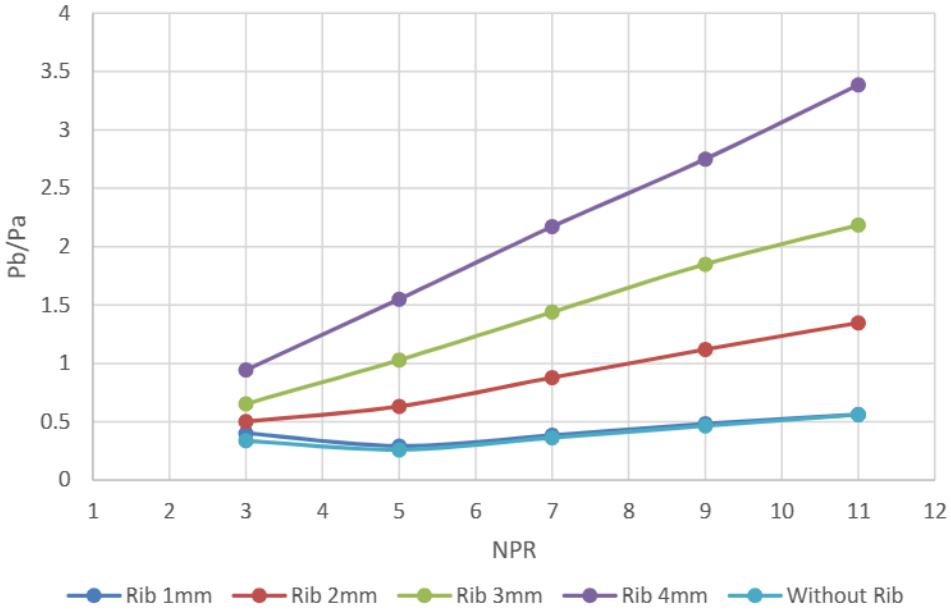


(d) L/D = 6

**Fig. 10.** Base Pressure Vs. NPR for various duct lengths

### *4.5 Base Pressure Results for Rib Location 3D*

For the farthest rib location of 66 mm from the base, the findings of this study are shown in Figure 11(a) to Figure 11(c), with rib radii 1 mm to 4 mm and NPRs ranging from 3 to 11. As discussed, the 1 mm rib and without control results show similar trends for other rib locations. As expected, the base pressure ratio is the maximum for a 4 mm rib radius at NPR = 11, with the highest level of under-expansion. For this case, the base pressure ratios for different rib radii range from 2 mm, 3 mm, and 4 mm are 1.5, 2.4, and 4.0, except for minor variations for duct lengths in L = 3D to 6D.

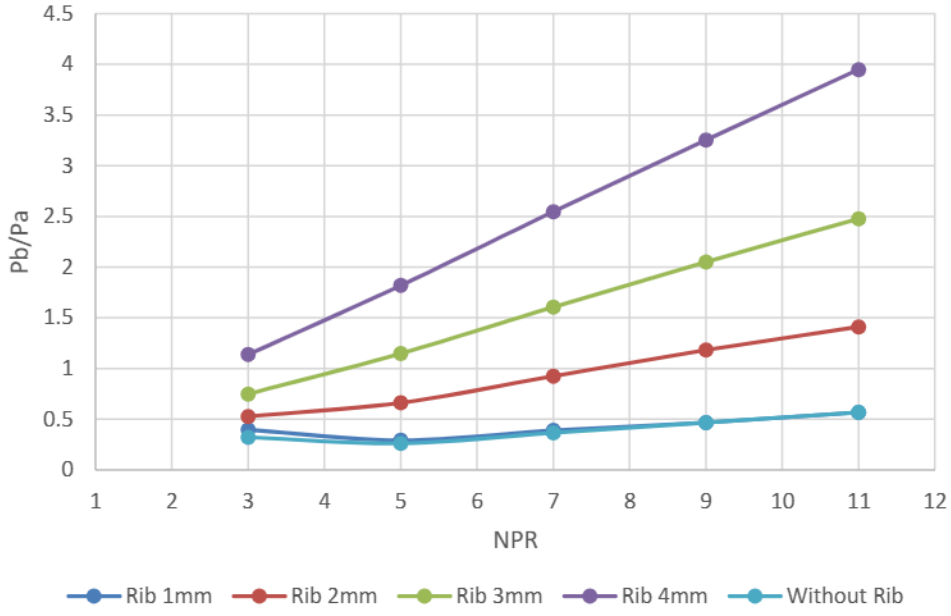
4.5
4
3.5
3
2.5
2
1.5
1
0.5
0
Pb/Pa
1
2
3
4
5
6
7
8
9
10
11
12
NPR
Rib 1mm
Rib 2mm
Rib 3mm
Rib 4mm
Without Rib

(a) L/D = 4

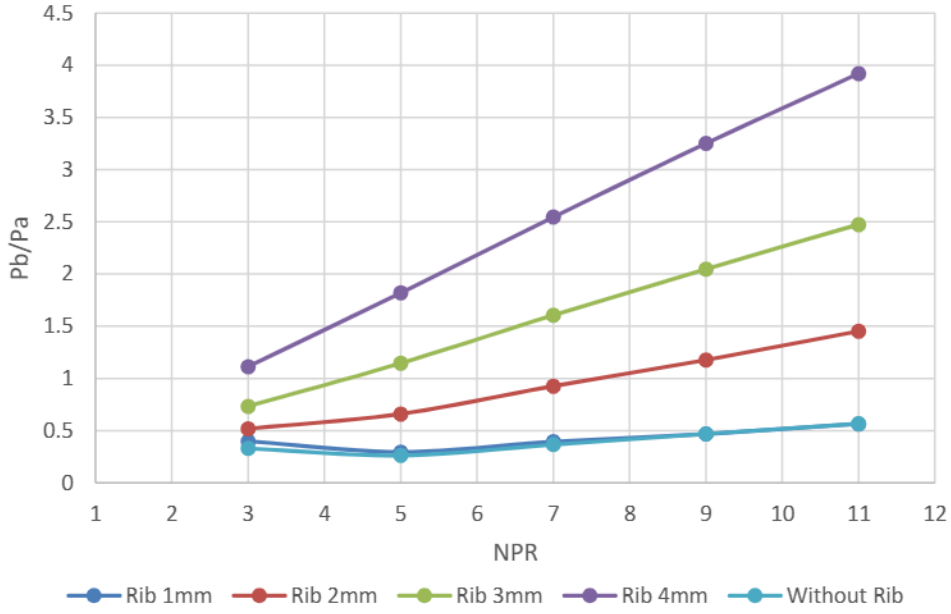
4.5
4
3.5
3
2.5
2
1.5
1
0.5
0
Pb/Pa
1
2
3
4
5
6
7
8
9
10
11
12
NPR
Rib 1mm
Rib 2mm
Rib 3mm
Rib 4mm
Without Rib

(b) L/D = 5

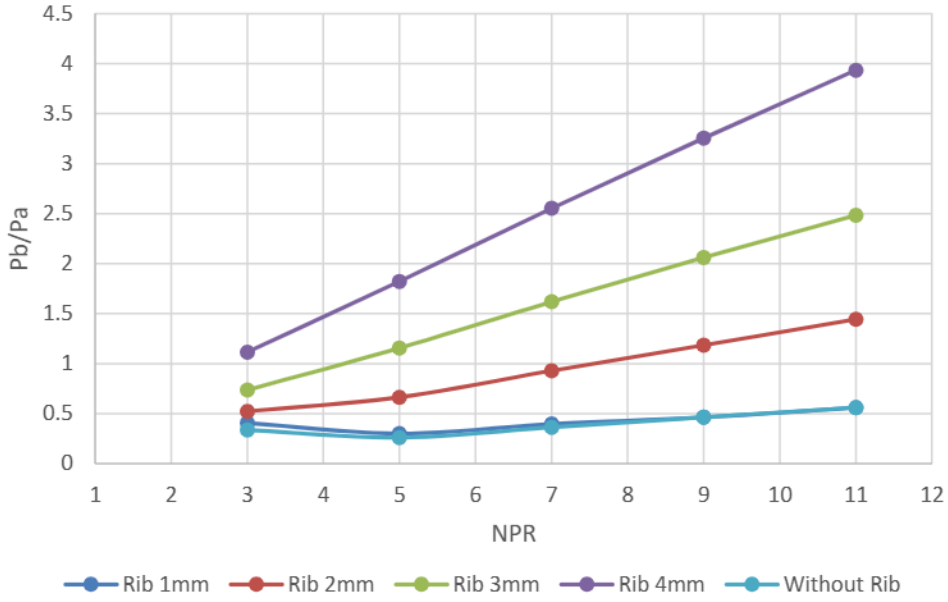


(c) L/D = 6

**Fig. 11.** Base Pressure Vs. NPR for various duct lengths

### *4.6 Pressure Contours*

Figure 12(a) to Figure 12(c) show pressure contours corresponding to a rib diameter of 4 mm, a nozzle pressure ratio (NPR) of 5, and a rib placement at 1D downstream. The outcomes are shown for various duct length-to-diameter (L/D) ratios of 2, 4, and 6. The pressure contours describe how the base pressure distribution fluctuates with differing L/D ratios. At L/D = 2, the base pressure region demonstrates moderate separation but exhibits lower reattachment. Conversely, at L/D = 4, a more stabilized flow reattachment occurs, accompanied by diminished flow separation, indicating an enhanced base pressure recovery. Notably, when L/D = 6, the pressure contours reveal further evolution, showcasing an improved base pressure and reduced recirculation zones. These findings imply that extended ducts (higher L/D ratios) and careful rib placements intensely affect flow reattachment and base pressure.

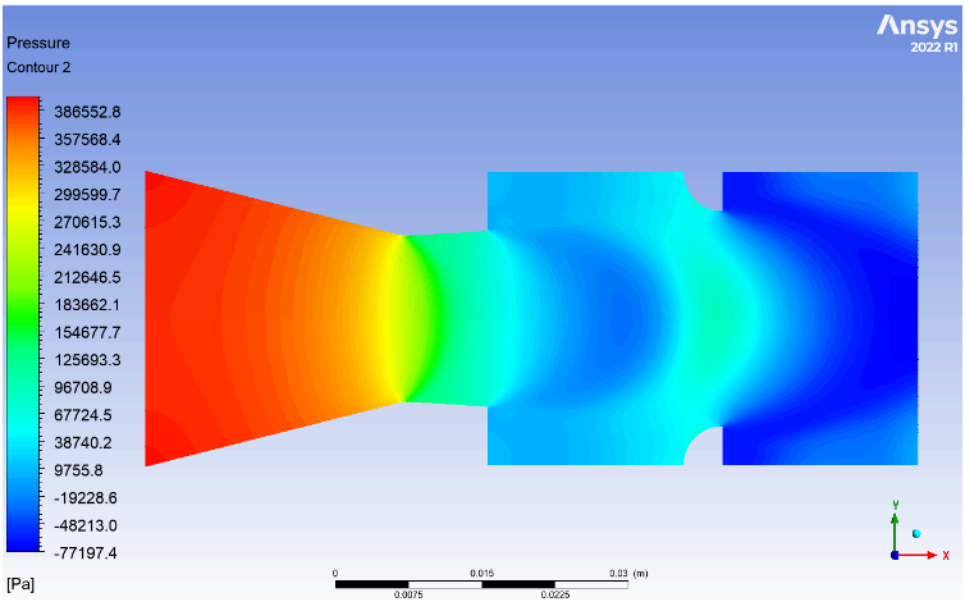


(a) L/D = 2

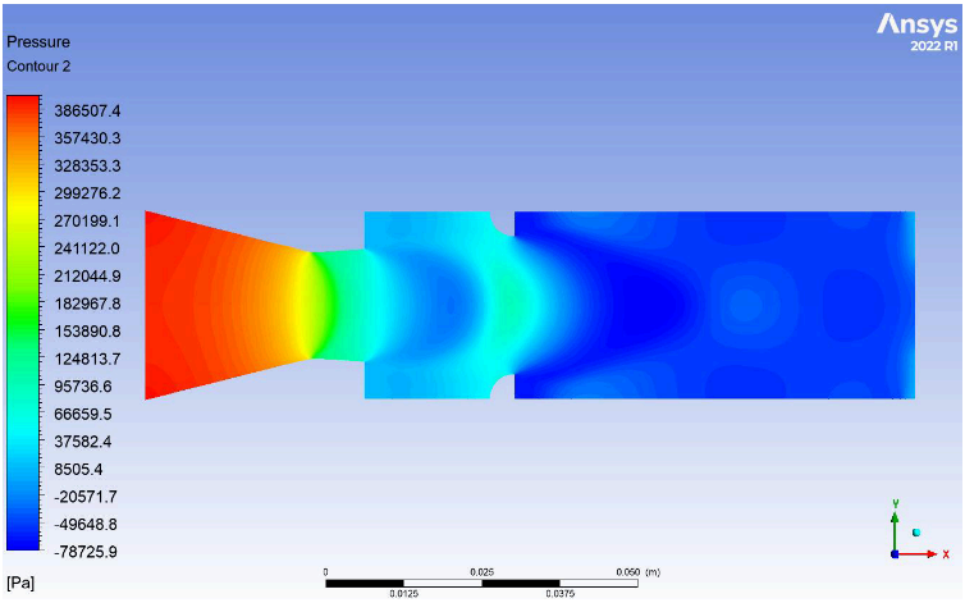


(b) L/D = 4

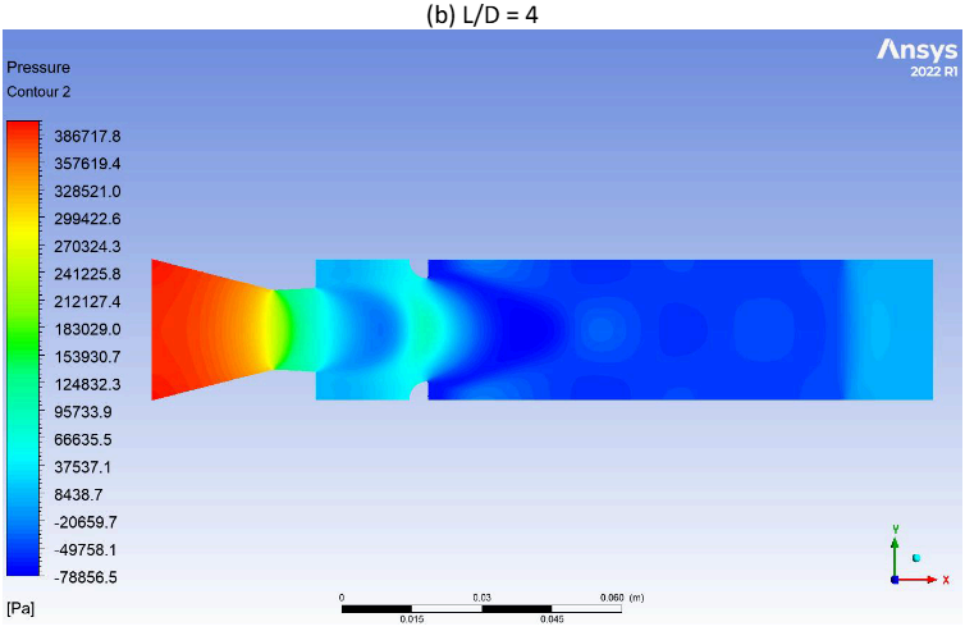


(c) L/D = 6

**Fig. 12.** Pressure Contours for Rib Diameter 4 mm, NPR=5 and Rib location at 1D

### *4.7 Velocity Contours*

Figure 13(a) to Figure 13(c) show the velocity contours corresponding to a rib diameter of 4 mm, a nozzle pressure ratio (NPR) of 5, and a rib location at 1D. When L/D = 2, the duct length is twice the diameter. The flow pattern reveals a separation region near the base, accompanied by conspicuous recirculation zones. The rib's presence significantly affects the flow; however, reattachment remains a work in progress downstream. When L/D = 4, the recirculation region propagates further downstream, demonstrating enhanced flow reattachment relative to L/D = 2. When L/D = 6, the flow stabilizes more efficiently, and the reattachment point becomes distinctly defined. The velocity contours exhibit diminished separation and enhanced flow uniformity downstream. This observation suggests that the elongated duct length facilitates more effective flow control when employing a rib.

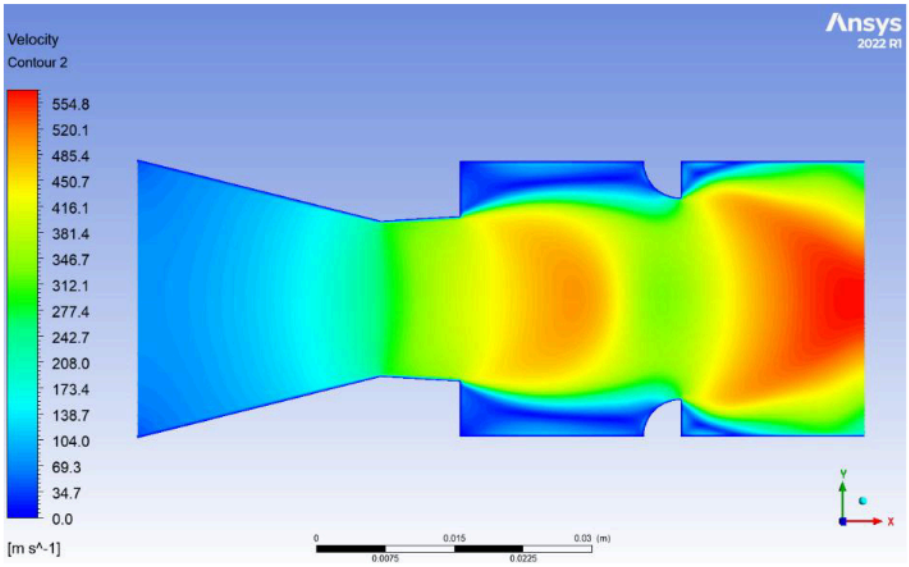


(a) L/D = 2

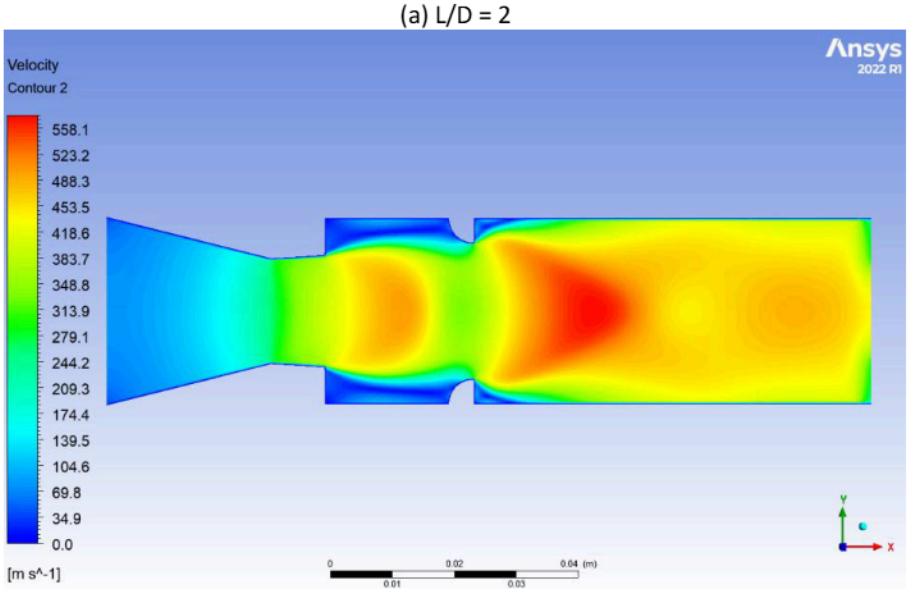


(b) L/D = 4

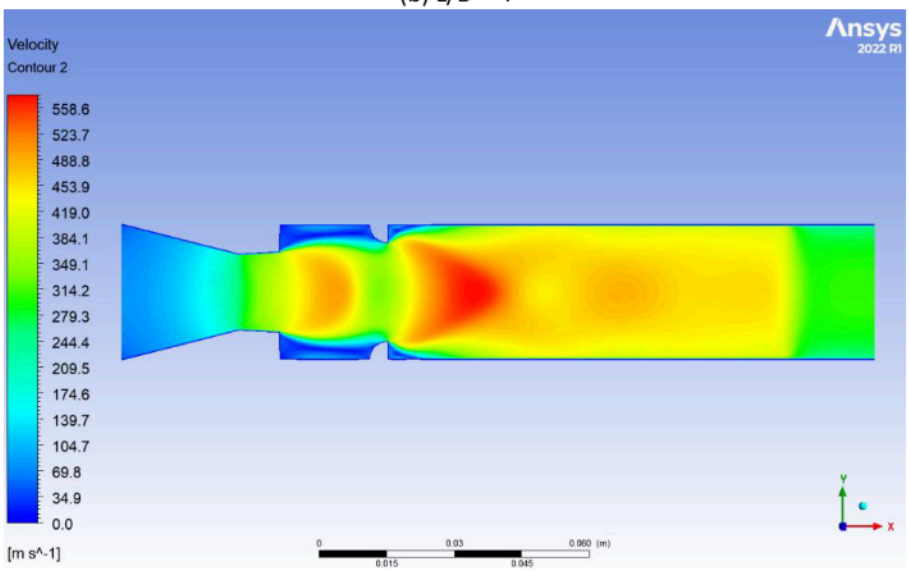


(c) L/D = 6

**Fig. 13.** Velocity Contours for Rib Diameter 4 mm, NPR=5 and Rib location at 1D

### *4.8 Velocity Streamlines*

Figure 14(a) to Figure 14(c) show the velocity streamlines for a rib diameter of 4 mm, a nozzle pressure ratio (NPR) of 5, and a rib location at 1D. When L/D = 2, the flow pattern reveals a prominent separation region near the base. When L/D = 4, the recirculation region propagates further downstream, demonstrating enhanced flow reattachment. When L/D = 6, the flow stabilizes more efficiently, and the reattachment point becomes distinctly defined.

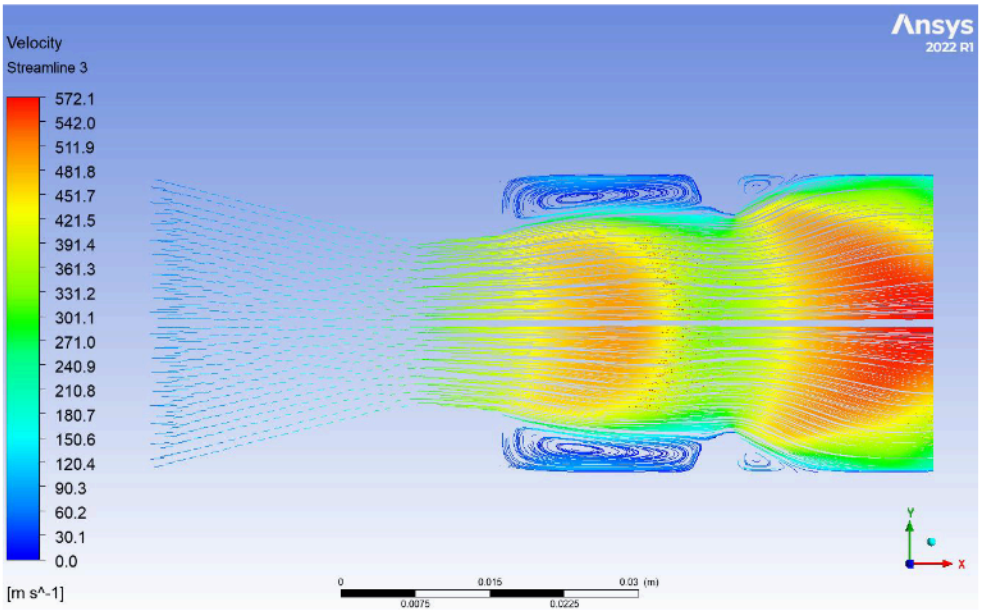


(a) L/D = 2

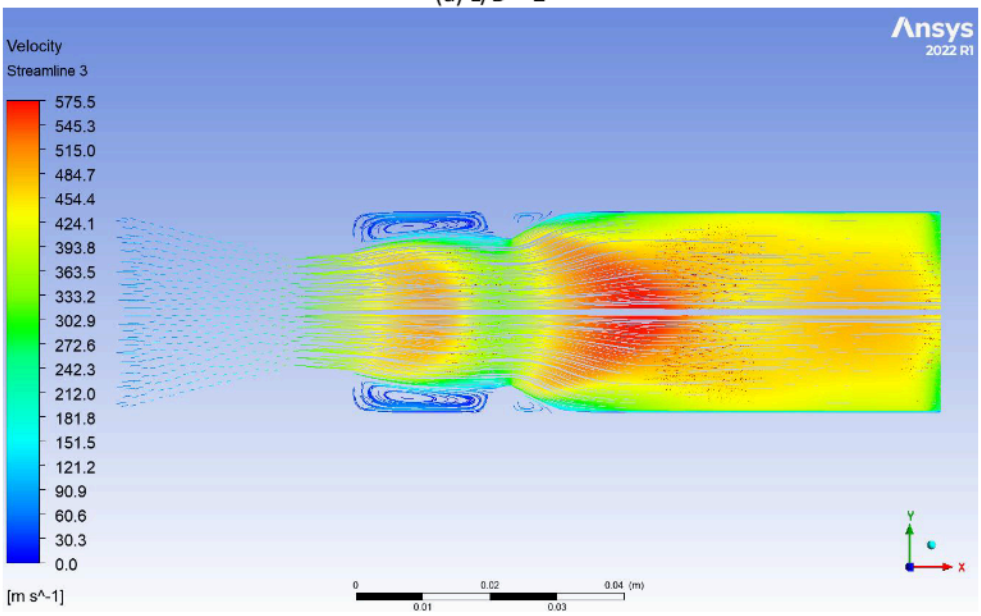


(b) L/D = 4

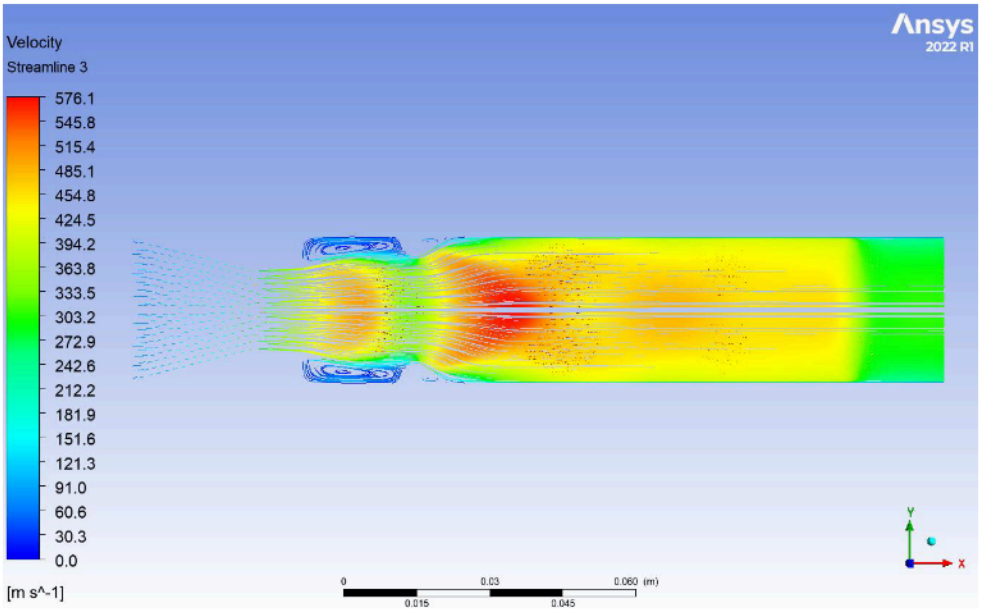


(c) L/D = 6

**Fig. 14.** Velocity Streamlines for Rib Diameter 4 mm, NPR=5 and Rib location at 1D

## 5. Conclusions

Based on the discussions in the previous section, we may draw the following conclusions: when ribs are located very close to the base recirculation region for the most petite duct length of 22 mm, there is a decline in the base pressure; however, there is no such trend for larger rib radius. When the ribs are located 11 mm from the base area, even a 1 mm rib radius has a significant role in fixing the base pressure values. There is a linear increase in the base pressure for all the rib radii, and this pattern continues for the rib location at 22 mm from the base. For this rib placement at 22 mm, the rib of 1 mm radius and without control, the base pressure values are identical, and this pattern holds suitable for all other rib locations of the present study. When ribs are located at a distance of 33 mm, 44 mm, and 66 mm, there is a continuous rise in the base pressure with the movement of the ribs towards the downstream, and these locations seem to be very close to the reattachment point. Therefore, depending on the user's requirements, one can decide to decrease the suction in the base recirculation zone and freeze the rib radius, rib location, and level of expansion for optimum control system performance. Based on the deliberation, it can concluded that the control is effective when jets are under-expanded and, more so, under the influence of adverse pressure gradient across the nozzle, the flow control mechanism becomes ineffective. Hence, these results reiterate that the effectiveness is directly associated with the expansion level and a strong function of the nozzle pressure ratio. In this case, NPR is an essential parameter in regulating the base pressure and, hence, the base drag.

## References

[1] Pathan, Khizar Ahmed, Prakash S. Dabeer, and Sher Afghan Khan. "Effect of nozzle pressure ratio and control jets location to control base pressure in suddenly expanded flows." *Journal of Applied Fluid Mechanics* 12, no. 4 (2019): 1127-1135. https://doi.org/10.29252/jafm.12.04.29495

[2] Pathan, Khizar Ahmed, Syed Ashfaq, Prakash S. Dabeer, and Sher Afgan Khan. "Analysis of Parameters Affecting Thrust and Base Pressure in Suddenly Expanded Flow from Nozzle." *Journal of Advanced Research in Fluid Mechanics and Thermal Sciences* 64, no. 1 (2019): 1-18.

[3] Fiqri, Muhammad Ikhwan, Khizar Ahmed Pathan, and Sher Afghan Khan. "Control of Suddenly Expanded Flow with Cavity at Sonic Mach Number." In *International Conference on Advances in Heat Transfer and Fluid Dynamics*, pp. 3-15. Singapore: Springer Nature Singapore, 2022. https://doi.org/10.1007/978-981-99-7213-5_1

[4] Asadullah, Mohammed, Sher Afghan Khan, Waqar Asrar, and E. Sulaeman. "Low-cost base drag reduction technique." *International Journal of Mechanical Engineering and Robotics Research* 7, no. 4 (2018): 428-432. https://doi.org/10.18178/ijmerr.7.4.428-432

[5] Pathan, Khizar A., Prakash S. Dabeer, and Sher A. Khan. "Enlarge duct length optimization for suddenly expanded flows." *Advances in Aircraft and Spacecraft Science* 7, no. 3 (2020): 203-214.

[6] Pathan, Khizar Ahmed, Prakash S. Dabeer, and Sher Afghan Khan. "Influence of expansion level on base pressure and reattachment length." *CFD Letters* 11, no. 5 (2019): 22-36.

[7] Azami, Muhammed Hanafi, Mohammed Faheem, Abdul Aabid, Imran Mokashi, and Sher Afghan Khan. "Inspection of supersonic flows in a CD nozzle using experimental method." *International Journal of Recent Technology and Engineering* 8, no. 2S3 (2019): 996-999. https://doi.org/10.35940/ijrte.B1186.0782S319

[8] Pathan, Khizar Ahmed, Zakir Ilahi Chaudhary, Ajaj Rashid Attar, Sher Afghan Khan, and Ambareen Khan. "Optimization of Nozzle Design for Weight Reduction using Variable Wall Thickness." *Journal of Advanced Research in Fluid Mechanics and Thermal Sciences* 112, no. 2 (2023): 86-101. https://doi.org/10.37934/arfmts.112.2.86101

[9] Azami, Muhammed Hanafi, Mohammed Faheem, Abdul Aabid, Imran Mokashi, and Sher Afghan Khan. "Experimental research of wall pressure distribution and effect of micro jet at Mach 1.5." *International Journal of Recent Technology and Engineering* 8, no. 2S3 (2019): 1000-1003. https://doi.org/10.35940/ijrte.B1187.0782S319

[10] Khan, Sher Afghan, Abdul Aabid, and Ahamed Saleel Chandu Veetil. "Influence of micro-jets on the flow development in the enlarged duct at supersonic Mach number." *International Journal of Mechanical and Mechatronics Engineering* 19, no. 1 (2019): 70-82.

[11] Khan, Sher Afghan, and E. Rathakrishnan. "Active control of suddenly expanded flows from unde-expanded nozzles-Part II." *International Journal of Turbo and Jet Engines* 22, no. 3 (2005): 163-184. https://doi.org/10.1515/TJJ.2005.22.3.163

[12] Shaikh, Javed S., Krishna Kumar, Khizar A. Pathan, and Sher A. Khan. "Analytical and computational analysis of pressure at the nose of a 2D wedge in high speed flow." *Advances in Aircraft and Spacecraft Science* 9, no. 2 (2022): 119-130.

[13] Shamitha, Shamitha, Asha Crasta, Khizer Ahmed Pathan, and Sher Afghan Khan. "Numerical simulation of surface pressure of a wedge at supersonic Mach numbers and application of design of experiments." *Journal of Advanced Research in Applied Mechanics* 101, no. 1 (2023): 1-18. https://doi.org/10.37934/aram.101.1.118

[14] Shamitha, Shamitha, Asha Crasta, Khizar Ahmed Pathan, and Sher Afghan Khan. "Analytical and Numerical Simulation of Surface Pressure of an Oscillating Wedge at Hypersonic Mach Numbers and Application of Taguchi's Method." *Journal of Advanced Research in Applied Sciences and Engineering Technology* 30, no. 1 (2023): 15-30. https://doi.org/10.37934/araset.30.1.1530

[15] Shaikh, Javed Shoukat, Khizar Ahmed Pathan, Krishna Kumar, and Sher Afghan Khan. "Effectiveness of Cone Angle on Surface Pressure Distribution along Slant Length of a Cone at Hypersonic Mach Numbers." *Journal of Advanced Research in Fluid Mechanics and Thermal Sciences* 104, no. 1 (2023): 185-203. https://doi.org/10.37934/arfmts.104.1.185203

[16] Shaikh, Javed S., Krishna Kumar, Khizar A. Pathan, and Sher A. Khan. "Computational analysis of surface pressure distribution over a 2D wedge in the supersonic and hypersonic flow regimes." *Fluid Dynamics & Materials Processing* 19, no. 6 (2023). https://doi.org/10.32604/fdmp.2023.025113

[17] Khan, Sher Afghan, M. A. Fatepurwala, and K. N. Pathan. "CFD analysis of human-powered submarine to minimize drag." *International Journal of Mechanical and Production Engineering Research and Development (IJMPERD)* 8, no. 3 (2018): 1057-1066. https://doi.org/10.24247/ijmperdjun2018111

[18] Pathan, Khizar A., Sher A. Khan, N. A. Shaikh, Arsalan A. Pathan, and Shahnawaz A. Khan. "An investigation of boattail helmet to reduce drag." *Advances in Aircraft and Spacecraft Science* 8, no. 3 (2021): 239.

[19] Fakhruddin, Ahmad 'Afy Ahmad, Fharukh Ahmed Ghasi Mahaboobali, Ambareen Khan, Mohammad Nishat Akhtar, Sher Afghan Khan, and Khizar Ahmad Pathan. "Analysis of Base Pressure Control with Ribs at Mach 1.2 using CFD Method." *Journal of Advanced Research in Fluid Mechanics and Thermal Sciences* 123, no. 1 (2024): 108-143. https://doi.org/10.37934/arfmts.123.1.108143

[20] Khan, Ambareen, Parvathy Rajendran, Junior Sarjit Singh Sidhu, S. Thanigaiarasu, Vijayanandh Raja, and Qasem Al-Mdallal. "Convolutional neural network modeling and response surface analysis of compressible flow at sonic and supersonic Mach numbers." *Alexandria Engineering Journal* 65 (2023): 997-1029. https://doi.org/10.1016/j.aej.2022.10.006

[21] Khan, Ambareen, Parvathy Rajendran, Junior Sarjit Singh Sidhu, and Mohsen Sharifpur. "Experimental investigation of suddenly expanded flow at sonic and supersonic Mach numbers using semi-circular ribs: a comparative study

between experimental, single layer, deep neural network (SLNN and DNN) models." *The European Physical Journal Plus* 138, no. 4 (2023): 314. https://doi.org/10.1140/epjp/s13360-023-03853-1

[22] Chaudhari, Pavan Bhaskar, Rachayya Arakerimath, Khizar Ahmed Pathan, and Sher Afghan Khan. "Comparative Experimental Analysis and Performance Optimization of Single-Cylinder DI and HCCI Engine with Series Catalytic Converters." *Journal of Advanced Research in Fluid Mechanics and Thermal Sciences* 121, no. 1 (2024): 173-187. https://doi.org/10.37934/arfmts.121.1.173187

[23] Jain, Yogeshkumar, Vijay Kurkute, Sagar Mane Deshmukh, Khizar Ahmed Pathan, Ajaj Rashid Attar, and Sher Afghan Khan. "The Influence of Plate Fin Heat Sink Orientation under Natural Convection on Thermal Performance: An Experimental and Numerical Study." *Journal of Advanced Research in Fluid Mechanics and Thermal Sciences* 114, no. 2 (2024): 118-129. https://doi.org/10.37934/arfmts.114.2.118129

[24] Khalil, Shaikh Sohel Mohd, Rai Sujit Nath Sahai, Nitin Parashram Gulhane, Khizar Ahmed Pathan, Ajaj Rashid Attar, and Sher Afghan Khan. "Experimental Investigation of Local Nusselt Profile Dissemination to Augment Heat Transfer under Air Jet Infringements for Industrial Applications." *Journal of Advanced Research in Fluid Mechanics and Thermal Sciences* 112, no. 2 (2023): 161-173. https://doi.org/10.37934/arfmts.112.2.161173

[25] Shaikh, Sohel Khalil, Khizar Ahmed Pathan, Zakir Ilahi Chaudhary, B. G. Marlpalle, and Sher Afghan Khan. "An investigation of three-way catalytic converter for various inlet cone angles using CFD." *CFD Letters* 12, no. 9 (2020): 76-90. https://doi.org/10.37934/cfdl.12.9.7690

[26] Shaikh, Sohel Khalil, Khizar Ahmed Pathan, Zakir Ilahi Chaudhary, and Sher Afghan Khan. "CFD analysis of an automobile catalytic converter to obtain flow uniformity and to minimize pressure drop across the monolith." *CFD Letters* 12, no. 9 (2020): 116-128. https://doi.org/10.37934/cfdl.12.9.116128

[27] Kale, Dipak, Rachayya Arakerimath, Khizar Ahmed Pathan, and Sher Afghan Khan. "Investigation on Water Erosion Behavior of Ti-based Metal Matrix Composite: Experimental Approach." *Journal of Advanced Research in Fluid Mechanics and Thermal Sciences* 122, no. 2 (2024): 71-82. https://doi.org/10.37934/arfmts.122.2.7182

[28] Sheikh, Fahim Rahim, Suresh Pandurang Deshmukh, Purushottam Ardhapurkar, Khizar Ahmed Pathan, Sohel Khalil Shaikh, and Sher Afghan Khan. "Modeling and Experimental Validation of NePCM-Nanofluid-Based PVT System." *Journal of Advanced Research in Fluid Mechanics and Thermal Sciences* 122, no. 1 (2024): 205-222. https://doi.org/10.37934/arfmts.122.1.205222

[29] Khan, Ambareen, Abdul Aabid, Sher Afghan Khan, Mohammad Nishat Akhtar, and Muneer Baig. "Comprehensive CFD analysis of base pressure control using quarter ribs in sudden expansion duct at sonic Mach numbers." *International Journal of Thermofluids* 24 (2024): 100908. https://doi.org/10.1016/j.ijft.2024.100908

[30] Khan, Ambareen, Sher Afghan Khan, Vijayanandh Raja, Abdul Aabid, and Muneer Baig. "Effect of ribs in a suddenly expanded flow at sonic Mach number." *Heliyon* 10, no. 9 (2024). https://doi.org/10.1016/j.heliyon.2024.e30313

[31] Khan, Ambareen, Sher Afghan Khan, Mohammed Nishat Akhtar, Abdul Aabid, and Muneer Baig. "Base Pressure Control with Semi-Circular Ribs at Critical Mach Number." *Fluid Dynamics & Materials Processing* 20, no. 9 (2024). https://doi.org/10.32604/fdmp.2024.049368

[32] Nurhanis, Tun, Ambareen Khan, Mohammad Nishat Akhtar, and Sher Afghan Khan. "Control of Base Pressure at Supersonic Mach Number in a Suddenly Expanded Flow." *Journal of Advanced Research in Fluid Mechanics and Thermal Sciences* 109, no. 1 (2023): 210-225. https://doi.org/10.37934/arfmts.109.1.210225

[33] Khan, Ambareen, Nurul Musfirah Mazlan, and Mohd Azmi Ismail. "Velocity Distribution and Base Pressure Analysis of Under Expanded Nozzle Flow at Mach 1.0." *Journal of Advanced Research in Fluid Mechanics and Thermal Sciences* 92, no. 1 (2022): 177-189. https://doi.org/10.37934/arfmts.92.1.177189

[34] Khan, Ambareen, Nurul Musfirah Mazlan, and Ervin Sulaeman. "Effect of Ribs as Passive Control on Base Pressure at Sonic Mach Numbers." *CFD Letters* 14, no. 1 (2022): 140-151. https://doi.org/10.37934/cfdl.14.1.140151

[35] Khan, Ambareen, Mohd Azmi Ismail, and Nurul Musfirah Mazlan. "Numerical Simulation of Suddenly Expanded Flow from Converging Nozzle at Sonic Mach Number." In *Proceedings of International Conference of Aerospace and Mechanical Engineering 2019: AeroMech 2019*, 20-21 November 2019, Universiti Sains Malaysia, Malaysia, pp. 349-359. Springer Singapore, 2020. https://doi.org/10.1007/978-981-15-4756-0_29

[36] Khan, Ambareen, Nurul Musfirah Mazlan, and Mohd Azmi Ismail. "Analysis of flow through a convergent nozzle at Sonic Mach Number for Area Ratio 4." *Journal of Advanced Research in Fluid Mechanics and Thermal Sciences* 62, no. 1 (2019): 66-79.

[37] Khan, Ambareen, Nurul Musfirah Mazlan, Mohd Azmi Ismail, and Mohammad Nishat Akhtar. "Experimental and numerical simulations at sonic and supersonic Mach numbers for area ratio 7.84." *CFD Letters* 11, no. 5 (2019): 50-60.

[38] Rathakrishnan, E. "Effect of ribs on suddenly expanded flows." *AIAA Journal* 39, no. 7 (2001): 1402-1404. https://doi.org/10.2514/2.1461